Controls on conduit magma flow dynamics during lava dome building eruptions

O. Melnik[1] and R. S. J. Sparks

Research Centre for Environmental and Geophysical Flows and Department of Earth Sciences, University of Bristol, Bristol, UK

Received 18 May 2004; revised 15 October 2004; accepted 7 December 2004; published 23 February 2005.

[1] Lava dome eruptions commonly display fairly regular alternations between periods of high and low or no activity with timescales typically of weeks to years and sudden transitions between effusive and explosive activity. We develop a transient model of the magma flow in a volcanic conduit from an open-system magma chamber with continuous replenishment. The model incorporates gas exsolution, bubble growth, gas escape through the magma, and decompression-induced crystallization and considers variations in magma temperature, water content, conduit diameter, phenocryst size, chamber volume, and magma rheology. Calculations show the presence of periodic variations in discharge rate due to the transition from a stable regime, when discharge rate is low and crystals grow efficiently leading to high magma viscosity, to another stable state, when discharge rate is high and crystallization is negligible. The difference in discharge rates between these regimes can be several orders of magnitude. Periods are similar to the observed timescales and mainly depend on the chamber volume. The system shows strongly nonlinear responses to the variation of governing parameters. If magma has a Bingham rheology pauses in discharge rate occur between peaks of discharge and the peaks are much higher than for the case of Newtonian rheology. Large changes in discharge rate and eruptive behavior can occur as the consequence of small changes in magma temperature, water content, phenocryst size distribution, or conduit diameter. The system can fluctuate between low and high discharge rates with transitions to explosive activity.

Citation: Melnik, O., and R. S. J. Sparks (2005), Controls on conduit magma flow dynamics during lava dome building eruptions, *J. Geophys. Res.*, *110*, B02209, doi:10.1029/2004JB003183.

1. Introduction

[2] Lava dome eruptions are an important style of volcanism. The eruptions can be long-lived, lasting many years or even decades [*Newhall and Melson*, 1983]. Dome-building eruptions are commonly associated with hazardous phenomena, including pyroclastic flows generated by dome collapses, explosive eruptions and volcanic blasts. Dome-building eruptions can also contribute to edifice instability and sector collapse, as occurred on Montserrat on 26 December 1997 [*Sparks and Young*, 2002]. Lava dome activity can sometimes precede or follow major explosive eruptions; the eruption of Pinatubo in 1991 is an example of the former [*Hoblitt et al.*, 1996], and the eruption of Mount St. Helens (1980–1986) is an example of the latter [*Swanson and Holcomb*, 1990].

[3] Several lava dome eruptions have been documented in detail and show quite complex behaviors. Substantial fluctuations in magma discharge rate have been documented. In some cases these fluctuations can be quite regular (nearly periodic) as in the extrusion of lava in 1980–1982 on Mount St. Helens [*Swanson and Holcomb*, 1990] and in the 1922–2002 activity of the Santiaguito lava dome, Guatemala [*Harris et al.*, 2002]. In these cases, periods of high discharge rate alternate with longer periods of low discharge rate or no effusion. In some volcanoes, such as Shiveluch, Kamchatka, the intervals of no effusion are so long compared with the periods of dome growth that the latter have been described as separate eruptions of the volcano rather than episodes of the same eruption. Other dome-building activity can be nearly continuous and fairly steady as in Mount St. Helens in 1983 [*Swanson and Holcomb*, 1990] and at the Soufrière Hills between November 1999 and July 2003. In yet other cases the behavior can be more complex with quite sudden changes in magma discharge rate which cannot be related to any well-defined regularity or pattern. For example, the discharge rate of the Soufrière Hills Volcano more than doubled in May 1997 from a typical rate of 2–3 m^3 s^{-1} in the period April 1996 to April 1997 to a typical rate of 7–8 m^3 s^{-1} in the period May 1997 to March 1998 [*Sparks et al.*, 1998].

[4] Pauses during lava dome building eruptions are quite common. For example, during the dome growth on Mount

[1] Also at Institute of Mechanics, Moscow State University, Moscow, Russia.

0148-0227/05/2004JB003183$09.00

St Helens there were 9 pulses of dome growth with a period of ~74 days with a duration of 1–7 days and no growth in between [*Swanson and Holcomb*, 1990]. Soufrière Hills Volcano Montserrat experienced a long (20 months) pause in extrusion after the first episode of growth [*Norton et al.*, 2002]. On Shiveluch volcano in Kamchatka episodes of the dome growth occurred in 1980, 1993 and 2000 after a major explosion in 1964 [*Fedotov et al.*, 2001]. Each episode of dome growth began with discharge rate increasing in the first few weeks to peaks of 8–15 m^3 s^{-1} with gradual decline in discharge rate over the following a year. In between the episodes very minimal activity was recorded.

[5] Fluctuations in discharge rate have been documented on a variety of timescales from both qualitative and quantitative observations. Several lava dome eruptions are characterized by extrusion of multiple lobes and flow units [*Nakada et al.*, 1999; *Watts et al.*, 2002]. In the case of the Soufrière Hills Volcano, extrusions of shear lobes can be related to surges in discharge rate and are associated with other geophysical changes such as onset of seismic swarms and marked changes in temporal patterns of ground tilt [*Voight et al.*, 1998, 1999; *Watts et al.*, 2002]. These surges in discharge rate have been fairly regular for substantial periods, occurring every 6 to 7 weeks [*Voight et al.*, 1999; *Sparks and Young*, 2002]. These surges are commonly associated with large dome collapses and pyroclastic flows and, in some cases, with the onset of periods of repetitive Vulcanian explosions [*Cole et al.*, 2002; *Druitt et al.*, 2002]. Consequently, the recognition of this pattern has become significant for forecasting activity for hazard assessment purposes. In the Soufrière Hills Volcano and Mount Pinatubo much shorter fluctuations in discharge rate have been recognized from cyclic variations in seismicity, ground tilt, gas fluxes and rockfall activity [*Denlinger and Hoblitt*, 1999; *Voight et al.*, 1999; *Watson et al.*, 2000]. This cyclic activity has typical periods in the range of 4 to 36 hours. Cyclic activity has been attributed to cycles of gas pressurization and depressurization with surges in dome growth related to degassing, rheological stiffening and stick-slip behavior [*Denlinger and Hoblitt*, 1999; *Melnik and Sparks*, 1999; *Voight et al.*, 1999; *Wylie et al.*, 1999].

[6] Dome eruptions can show transitions to explosive activity, which sometimes can be linked to surges in discharge rate. For example, in 1980 periodic episodes of lava dome extrusion on Mount St. Helens were initiated by explosive eruptions, which partly destroyed the dome that had been extruded in each previous extrusion episode [*Swanson and Holcomb*, 1990]. At Unzen Volcano a single Vulcanian explosive eruption occurred in June 1991 when the discharge rate of the dome was at its highest [*Nakada et al.*, 1999]. At the Soufrière Hills Volcano, repetitive series of Vulcanian explosions have occurred following large dome collapses in periods when magma discharge rates were the highest of the eruption [*Sparks et al.*, 1998; *Druitt et al.*, 2002]. In the case of Lascar Volcano, Chile, an intense plinian explosive eruption occurred on 18 and 19 April, 1993 after nine years of dome extrusion and occasional short-lived Vulcanian explosions [*Matthews et al.*, 1997].

[7] These observations of dome discharge rate variations on a variety of timescales and the inferences concerning pressurization processes highlight the need to understand the underlying dynamic controls. Research has increasingly focused on modeling studies of conduit flow dynamics during lava dome eruptions. *Sparks* [1997] identified rheological stiffening due to degassing and crystallization as a dominant effect on the pressurization of magma in the upper part of the conduits during lava dome eruptions. *Melnik and Sparks* [1999] developed a dynamical model of conduit flow in lava dome extrusions which took account of gas exsolution, gas escape by permeable flow, crystallization kinetics, and rheological variations in the magma due to these processes. This model drew attention to the nonlinear nature of conduit flows during magma ascent with strong feedbacks between processes. *Melnik and Sparks* [1999] established that large overpressures relative to lithostatic pressure of several MPa could be developed in the uppermost parts of volcanic conduits, which could account for shallow pressure sources inferred from ground deformation data and shallow seismicity, as well as explaining the propensity for excess pressures reaching sufficiently high values for explosive eruptions. They also showed that some conditions resulted in models showing multiple steady state solutions at fixed magma driving pressure. In such a system periodic behavior becomes possible. These models were largely applied to the lava dome eruption at the Soufrière Hills Volcano, Montserrat. *Melnik and Sparks* [2002] further developed the models for this eruption by improving the model for crystallization kinetics and magma permeability, and they explored how variations of the governing parameters such (as conduit diameter or magma chamber crystal content) controlled flow dynamics using quasi-static approach.

[8] *Barmin et al.* [2002] explored a simplified transient model of conduit flow, in which the viscosity variations were described as a step change when a critical crystal content is reached. This model also included the elasticity of the magma chamber walls, magma chamber size and input rate to the chamber as parameters. Pressure in the chamber could vary, in contrast to the models of *Melnik and Sparks* [1999, 2002] where chamber pressure was kept constant. Thus *Barmin et al.* [2002] were able to study the interplay of inputs and outputs from the chamber, pressure variation in the chamber and fluctuation of discharge rate. These models were able to simulate periodic patterns of lava dome extrusion similar to those observed in nature. In particular, they were able to simulate patterns of lava extrusion at Mount St. Helens in 1980–1986 [*Swanson and Holcomb*, 1990] and at Santiaguito, Guatemala in 1922–2002 [*Harris et al.*, 2002] using parameters either measured or inferred from observations. There were simplifications in this model with important effects not being taken into account. These include cross-conduit pressure variations [*Massol and Jaupart*, 1999], continuous rheological variations with crystal content, and variations in dome height [*Stasiuk et al.*, 1993]. Nevertheless, this approach enabled *Barmin et al.* [2002] to define some nondimensional parameters which have an important influence on flow dynamics. For example, one parameter, informally the "magma chamber pressure relaxation time," allowed a study of how magma chamber size controlled the timescale of periodic behavior.

[9] Nonlinear effects and bifurcations are well known in Chemical Engineering [*Aris*, 2000; *Scott*, 1994] as well as in geological systems [*Slezin*, 1984, 2003; *Jaupart and*

Table 1. Parameters Used in the Simulations

Notation	Description	Basic Value	Range
c_0	concentration of dissolved gas	5 wt%	4–7 wt%
C_f	solubility coefficient	4.1×10^{-6} Pa$^{-1/2}$	
C_m	specific heat	1.2×10^3 J kg^{-1} K^{-1}	
D	conduit diameter	30 m	20–50 m
E	rigidity of the rocks	3×10^{10} Pa	
I_0	maximum nucleation rate	3×10^{10} m^{-3} s^{-1}	
j		3.5	
k_0	permeability coefficients (equation (1f))	5×10^{-12} m^2	
L	length of the conduit	5 km	
L_*	latent heat of crystallization	3.5×10^6 J kg^{-1}	
Q_{in}	intensity of the influx	2 m^3 s^{-1}	
R	gas constant	460 J kg^{-1} K^{-1}	
R_{ph}	phenocryst size	5 mm	0.1–5 mm
T_{ch}	temperature in the magma chamber	850°C	825°–875°C
U_0	max growth rate	10^{-9} m s^{-1}	
V_{ch}	chamber volume	30 km^3	0.5–50 km^3
β_*		0.69	
β_{cr}	critical crystal content	0.65	
ΔT_i	max undercooling for nucleation	90°K	
ΔT_u	max undercooling for growth	60°K	
ε		8.6	
θ_0	parameters in viscosity function $\theta(\beta)$ (equation (14))	1.4	
μ_g	gas viscosity	1.5×10^{-5} Pa s	
ρ_c	density of crystals	2700 kg m^{-3}	
ρ_m	density of the melt phase	2300 kg m^{-3}	
τ_b	yield strength	0	0–0.2 MPa

Allegre, 1991; *Woods and Koyaguchi*, 1994; *Bonnefoi et al.*, 1995, 1999]. *Bonnefoi et al.* [1995, 1999] focused on magma chamber processes and have shown strong nonlinearity of the system. They demonstrated, for example, that crystallization kinetics can have large effects on the internal evolution of open-system magma chambers with small changes in parameters having large effects. Their work shows the possibility of multiple states of crystallization rate with sudden changes in resulting magma composition.

[10] In this paper we develop these models further to examine new effects and relax some of the simplifications of earlier models. We investigate a number of effects that were not fully explained or considered in previous studies [*Melnik and Sparks*, 1999; *Barmin et al.*, 2002; *Melnik and Sparks*, 2002]. We study effects of chamber size on the periodicity of dome eruptions and on conditions where steady stable flow rather then periodic or more complicated fluctuations of discharge rate can occur. The new model incorporates a more advanced treatment of crystallization kinetics based on the theoretical concepts given by *Hort* [1998] and calibrated by experimental studies in andesitic systems [*Couch et al.*, 2003]. In particular in the model we distinguish growth of phenocrysts formed in the magma chamber from crystallization of microlites during magma ascent. Previous models have assumed that magma is always Newtonian, so we study models of conduit flow assuming non-Newtonian rheology, with rheological properties being related to crystal content. Latent heat is released during the crystallization of ascending magma due to degassing and we show that this can have an important influence on the dynamics. These studies establish the strong sensitivity of eruptive behavior to small changes in volatile content and temperature in the magma chamber. These various explorations of parameter space and processes using a numerical modeling approach provide a more comprehensive picture of the underlying causes of variation in eruptive activity in lava dome eruptions, and provide a physical framework for interpreting observations, making forecasts and developing hazard assessments.

2. Physical Model of Conduit Flow During Lava Dome Building Eruptions

2.1. System of Equations

[11] We have modeled the ascent of magma along the conduit (given as x) from the chamber with the following 1-D equations:

$$\frac{\partial}{\partial t}\rho_m + \frac{\partial}{\partial x}\rho_m V = -G_{mc} - G_{ph} \qquad \frac{\partial}{\partial t}\rho_{ph} + \frac{\partial}{\partial x}\rho_{ph} V = G_{ph}$$
$$\frac{\partial}{\partial t}\rho_{mc} + \frac{\partial}{\partial x}\rho_{mc} V = G_{mc} \tag{1a}$$

$$\frac{\partial}{\partial t}\rho_d + \frac{\partial}{\partial x}\rho_d V = -J \qquad \frac{\partial}{\partial t}\rho_g + \frac{\partial}{\partial x}\rho_g V_g = J \tag{1b}$$

$$\frac{\partial}{\partial x}p = -\rho g - F_\mu \tag{1c}$$

$$V_g - V = -\frac{k(\alpha)}{\mu_g}\frac{\partial}{\partial x}p \tag{1d}$$

$$\rho C_m\left(\frac{\partial}{\partial t}T + V\frac{\partial}{\partial x}T\right) = L_*\left(G_{ph} + G_{mc}\right) \tag{1e}$$

$$\rho_m = \rho_m^0(1-\alpha)(1-\beta)(1-c); \quad \rho_{ph} = \rho_c^0(1-\alpha)\beta_{ph}$$
$$\rho_{mc} = \rho_c^0(1-\alpha)\beta_{mc}; \quad \beta = \beta_{ph} + \beta_{mc}$$
$$\rho_x = \rho_m^0(1-\alpha)(1-\beta)c; \quad \rho_g = \rho_g^0\alpha \tag{1f}$$
$$\rho = \rho_m + \rho_{ph} + \rho_{mc} + \rho_x + \rho_g$$
$$\alpha = \frac{4}{3}\pi a^3 n; \quad k(\alpha) = k_0\alpha^j; \quad \frac{\partial n}{\partial t} + \frac{\partial}{\partial x}nV = 0; \quad p = \rho_g^0 RT$$

where ρ_m, ρ_{ph}, ρ_{mc}, ρ_d, and ρ_g are the densities of melt, phenocrysts, microlites, dissolved and exsolved gas, respectively, ρ is the bulk density of erupting magma, superscript "0" on the density value means the density of a pure phase, subscript "c" is for the density of the crystal phase, α and β are volume concentrations of bubbles and crystals (phenocrysts and microlites being noted by β_{ph} and β_{mc}, respectively) in the condensed phase, V and V_g are the velocities of magma and gas, p is the pressure, c is the mass concentration of dissolved gas, $k(\alpha)$ is the permeability, R is the gas constant, T is the temperature, x is the vertical coordinate, $x = 0$, L corresponds to the top of the magma chamber and the top of the conduit, respectively, n is the number density of bubbles per unit volume, G_{ph}, G_{mc}, and J represent the mass transfer rates due to crystallization of phenocrysts and microlites and due to the gas exsolution, a is the bubble radius, F_μ is the force due to the conduit friction, C_m is the heat capacity of magma, and L_* is the latent heat of crystallization which is assumed to be constant. We use SI units throughout the paper with dimensions of the parameters being defined in Table 1.

[12] The system is a development of the model of *Melnik and Sparks* [1999, 2002] where steady state isothermal models for the conduit flow are presented. Equations (1a) and (1b) represent conservation of mass for melt and crystals (for phenocrysts and microlites) and dissolved and exsolved gas, respectively. Equation (1c) states the conservation of momentum for the mixture as a whole in which the inertial term is negligibly small. Equation (1d) is Darcy's law for the gas flow through the system of interconnected bubbles in which the gravity force acting on the gas phase can be neglected due to the low gas density. Equation (1e) is the thermal energy equation accounting for release of latent heat of crystallization. Equations (1f) are definitions of component densities, permeability-porosity relation, and conservation of the number density of bubbles.

2.2. Kinetics of Mass Transfer in Ascending Magma

[13] The kinetics of gas exsolution and degassing-induced crystallization are discussed in *Melnik and Sparks* [2002]. Following *Hort* [1998] crystal growth and nucleation rates were introduced as functions of undercooling, where effective liquidus temperature depends both on concentration of dissolved gas and amount of crystallized material [*Cashman and Blundy*, 2000].

$$G_{mc} = 3\sigma\rho_c^0(1-\beta)(1-\alpha)U(t)\int_0^t I(\omega)\left(\int_\omega^t U(\eta)d\eta\right)^2 d\omega \tag{2}$$

[14] Here I is the nucleation rate ($m^{-3}\ s^{-1}$), which defines the number of newly nucleated crystals per cubic meter per second, U is the linear crystal growth rate ($m\ s^{-1}$), and ω and η are integration parameters. This is an integral equation [*Hort*, 1998] which allows calculation of the mass flux due to crystallization. The outer integral in (2) determines the amount of crystals that appear in the time interval [0, t]. The internal integral shows the change of surface area for the same interval of time. By multiplying the integrals by $3\sigma U(t)$, where σ is a crystal shape factor ($\sigma = 1$ for a spherical crystal), we obtain the increase in volume. Both $U(t)$ and $I(t)$ are functions of magma undercooling. The theory of *Hort* [1998], developed by *Melnik and Sparks* [2002], accounts for the changes in magma liquidus temperature due to exsolution of water from the melt and changes in chemical composition of magma due to crystallization.

[15] Here we develop further the treatment of crystallization during magma ascent by distinguishing between phenocrysts that had formed in the chamber prior to eruption and microlites. The former can grow further during magma ascent and degassing. We can thus investigate the relative importance of overgrowth of existing phenocrysts and the nucleation of new crystals to form microphenocrysts and microlites during magma ascent under different conditions. We calibrate the parameters in equation (2) from the experimental studies of *Couch et al.* [2003], which examined the kinetics of crystallization induced by decompression and degassing in rhyolitic melts with compositions representative of the melt phases in andesites and dacites.

[16] We assume that all phenocrysts are spherical for simplicity (different shapes can be treated by introduction of a shape parameter) and have initial radius R_{ph} and number density N_{ph} in the condensed phase. Volume fraction of phenocrysts can be calculated as $\beta_{ph} = 4\pi R_{ph}^3 N_{ph}/3$ and total surface area S_{ph} is $4\pi R_{ph}^2 N_{ph}$. Increase in the volume of phenocrysts during time Δt can be calculated as

$$\beta_{ph}(t+\Delta t) = \beta_{ph}(t) + S_{ph}(t)U(t)\Delta t. \tag{3}$$

[17] After manipulations with the equation (3) using the definitions of β_{ph} and S_{ph} the expression for the phenocryst growth rate can be written as

$$G_{ph} = 3\left(\frac{4\pi N_{ph}\beta_{ph}^2}{3}\right)^{1/3}\rho_c^0 U(t)(1-\alpha)(1-\beta). \tag{4}$$

[18] Experimental data [*Hammer and Rutherford*, 2002; *Couch et al.*, 2003] place empirical constraints on the functions U and I. In these experiments the focus of study was on the crystallization of plagioclase feldspar, which is the major crystallizing phase during decompression of andesite and dacite magmas. Hereafter crystals are assumed to be feldspars in the model development. In the experiments of *Couch et al.* [2003] an initial rhyolitic melt composition was estimated for the magma chamber of the Soufrière Hills Volcano, Montserrat. The melt was saturated with water at a pressure of 160 MPa and temperature of 875°C, conditions close to but slightly below the liquidus (by ~10°C) for this composition. These experiments were carried out with constant temperature at a pressure range between 30 and 160 MPa. The pressure was decreased rapidly and maintained at a constant value for time periods

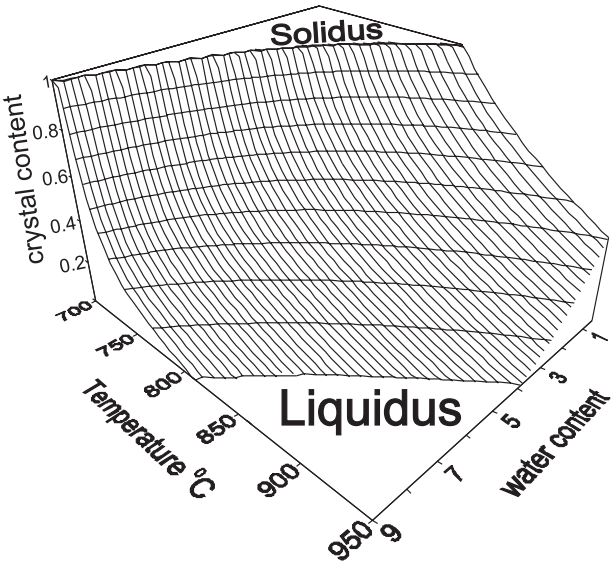

Figure 1. Equilibrium crystal content as a function of pressure and temperature calculated from equation (8) for the experimental conditions of *Couch et al.* [2003]. Areas where β_{eq} = 0 and 1 correspond to the conditions above liquidus and below solidus, respectively.

of 1, 4, 8, 24, 48, 120, 168 and 504 hours before quenching and analysis. *Hammer and Rutherford* [2002] studied a rhyolitic composition representative of the melt phase in the dacite pumice of Mount Pinatubo at 780°C with various decompressions from the initial pressure of 220 MPa. Total crystal content, crystal size and number density of crystals were measured in both experimental studies.

[19] We define U and I in a form after *Hort* [1998]:

$$I(T) = I_0 \exp\left(-\frac{\Delta G_t}{RT}\right)\exp\left(-\frac{\Delta G_c}{RT}\right);\quad \Delta G_c = \frac{16}{3}\pi\frac{\Sigma^3}{\Delta h_v^2}\frac{T_m^2}{T_m - T}$$
$$U(T) = U_0 \exp\left(-\frac{\Delta G_t}{RT}\right)\left[1 - \exp\left(-\frac{\Delta h_v (T_m - T)}{RT_m T}\right)\right] \quad (5)$$

where ΔG_t and ΔG_c are the activation energies of atomic diffusion and formation of a single nuclei, respectively; Δh_v is the enthalpy difference between the melt and the crystal, T is temperature, R is the universal gas constant, Σ is surface tension, and U_0, I_0 are constants. The first exponents (ΔG_t/RT) in (5) determine the rate of diffusion of components to the growing crystal. At the liquidus temperature (T_m) these rates are equal to zero and increase with undercooling. For some critical undercoolings $\Delta T_I = T_m - T$ and $\Delta T_u = T_m - T$ nucleation and growth rates, respectively, reach their maxima and decrease with further undercooling.

[20] The liquidus temperature changes during crystallization due to the progressive change in chemical composition of the melt. If magma temperature is constant after crystallization of a certain amount of crystals, the liquidus temperature of the remaining melt will become equal to the magma temperature and crystal growth will cease, corresponding to equilibrium conditions between melt and crystals. We term the volume fraction of crystals, which is at equilibrium with the melt, the equilibrium crystal content (β_{eq}). Values of β_{eq} can be determined from experiments of *Hammer and Rutherford* [2002] and *Couch et al.* [2003]. We will use parameterization for *Couch et al.* [2003] for the model. The best fit with experimental data is given by

$$\beta_{eq}(p, T = 875\,^\circ\mathrm{C}) = \beta_{ex}(p) = a_\beta + b_\beta \ln(p)^2 + c_\beta \ln(p)/p^2$$
$$a_\beta = 0.52;\ b_\beta = -1.78 \times 10^{-2};\ c_\beta = 22.88. \quad (6)$$

[21] To evaluate equilibrium crystal content for a different temperature we can use definitions of liquidus and solidus temperatures so that $\beta_{eq}(p, T_{liq}(p)) = 0$ and $\beta_{eq}(p, T_{sol}(p)) = 1$. Best fits for liquidus and solidus temperatures as functions of pressure for *Couch et al.* [2003] melt composition is given by

$$T_{liq,sol} = a_T + b_T \ln(p) + c_T \ln(p)^2 + d_T \ln(p)^3$$
$$\text{Liquidus: } a_T = 1465.4;\ b_T = -31.4;\ c_T = -2.8;\ d_T = -0.41$$
$$\text{Solidus: } a_T = 1252.2;\ b_T = -25.3;\ c_T = -11.9;\ d_T = 1.17. \quad (7)$$

[22] Here temperature is measured in Kelvin, pressure in MPa. An approximation of the equilibrium crystal content can be constructed as

$$\beta_{eq}(p, T) = \frac{A(p)\big(T - T_{liq}(p)\big)}{B(p) - T}. \quad (8)$$

[23] Here functions $A(p)$ and $B(p)$ must be found from the conditions $\beta_{eq}(p, T_{sol}(p)) = 1$ and $\beta_{eq}(p, T = 875°\mathrm{C}) = \beta_{ex}(p)$. The dependence of equilibrium crystal content on temperature and pressure is shown in Figure 1. Zones where β_{eq} = 0 and 1 correspond to temperatures above the liquidus and below the solidus.

[24] As β approaches β_{eq} magma undercooling tends to zero. We introduce variable $\Omega = 1 - \beta/\beta_{eq}$ so that at $\Omega = 1$ for $\beta = 0$ and $\Omega = 0$ for $\beta = \beta_{eq}$. The effective melting temperature can be represented by the expression

$$T_m = \big(T_{liq} - T\big)\Omega + T. \quad (9)$$

[25] Equation (9) gives zero undercooling for equilibrium conditions and the melting temperature is equal to the liquidus temperature for $\beta = 0$. This approach allows us to incorporate the change in chemical composition of the residual melt into crystal growth kinetics.

[26] From a mass balance $\rho_c\, d\beta/dt = G_{mc}$ the evolution of the system can be calculated. Preliminary calculations, using ((2), (5)–(9)) for the crystal growth and nucleation rates, resulted in a much more rapid increase in crystal content with time than the experimental data (symbols in Figure 2). This is due to activation energy of atomic diffusion ΔG_t remaining constant in the calculations. As crystallization proceeds the residual melt becomes more evolved and its viscosity increases, and diffusion accordingly decreases. We postulated that the decrease in diffusivity has a linear dependence on crystal content and,

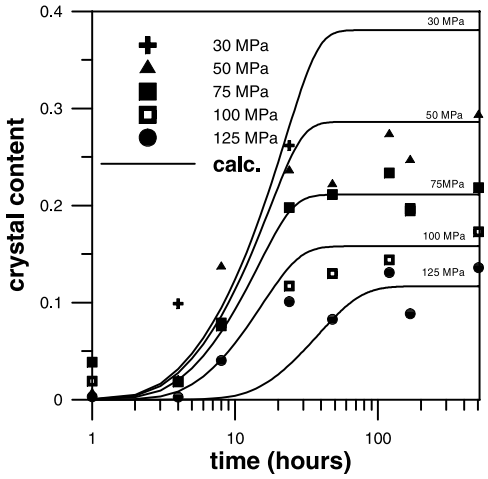

Figure 2. Comparison of calculated crystal content (equations (2) and (5)–(9)) with experimental data at 875°C from *Couch et al.* [2003]. Different symbols represent different final pressures for the experiments marked by numbers of final pressure.

therefore, multiplied both U and I by $(1 + \omega\beta)^{-1}$ where ω is a constant coefficient. Comparison of the calculated crystal content with the experimental results is shown in Figure 2. Calculated crystal content variations with time fit observations within the uncertainties of the experimental data for the whole range of experimental conditions. Best fit parameters are as follows: $U_0 = 3\ 10^{-9}$ m s^{-1}, $I_0 = 3\ 10^{10}$ m^{-3} s^{-1}, $\Delta T_I = 90$ K, $\Delta T_u = 60$ K, $\omega = 30$ for the case of the Soufrière Hills melt composition at 875°C.

[27] For the mass transfer of the gas (assumed to be water) between melt and bubbles we assumed that this happens quasi-statically, so that analytical solutions for the concentration gradient in a bubble shell [*Navon and Lyakhovski*, 1998] can be applied. The difference between the local pressure and internal pressure in the growing bubbles is not large for slowly ascending magma. We therefore neglect pressure disequilibrium, although we recognize that pressure disequilibrium might arise because of other processes, such as fast microlite crystallization [*Sparks*, 1997; *Stix et al.*, 1997] or when there is a sudden external pressure change (e.g., a dome collapse). Using these assumptions the mass flux due to the water exsolution can be calculated as

$$J = 4\pi a^2 n D \rho_m^0 \frac{c - c_{eq}}{a};\ c_{eq} = C_f\sqrt{p}. \tag{10}$$

[28] Here D and C_f are the diffusion and solubility coefficients, c and c_{eq} are the averaged and equilibrium concentrations of dissolved volatiles.

2.3. Rheology and Conduit Resistance

[29] In the case of Newtonian magma rheology the conduit friction force can be obtained from a classical Poiseuille solution for low Reynolds numbers $F_\mu = 32\mu V/d^2$, where d is a conduit diameter, and μ is the magma viscosity. High crystal or bubble content magmas may show non-Newtonian rheology. One possible non-Newtonian rheology is that of a Bingham material characterized by a yield strength τ_b [*Bingham*, 1922]. The stress-strain relation for this material is given by

$$\begin{aligned} \tau_{ij} &= \left(\mu + \frac{\tau_b}{\gamma}\right)\gamma_{ij} \Leftrightarrow \tau > \tau_b \\ \gamma_{ij} &= 0 \Leftrightarrow \tau \le \tau_b. \end{aligned} \tag{11}$$

[30] Here τ_{ij} and γ_{ij} are the stress and strain rate tensors, τ and γ are second invariants of corresponding tensors. According to this rheological law the material behaves linearly when applied stress is higher then a yield strength. No motion occurs if the stress is lower than a yield strength.

[31] Following *Loitsyansky* [1978] we can relate the average velocity in the pipe with the stress on the conduit wall τ_w.

$$V = \frac{1}{12}\frac{r}{\tau_w^3\mu}\left(\tau_b^4 + 3\tau_w^4 - 4\tau_b\tau_w^3\right). \tag{12}$$

[32] Here $r = d/2$ is the conduit radii. This form of equation gives an implicit relation between ascent velocity and pressure drop, and is not convenient to use. By introducing dimensionless variables $\Pi = \mu V/\tau_b r$ and $\Theta = \tau_w/\tau_b \ge 1$ relation (12) can be transformed into

$$\Theta^4 - \frac{1}{6}(8 + 3\Pi)\Theta^3 + \frac{1}{3} = 0. \tag{13}$$

[33] There are two asymptotic solutions of equation (13) for small and large values of Π:

$$\begin{aligned} \Theta_1 &= 1 + {}^1\!/_2\sqrt{\Pi},\quad \Pi \to 0 \\ \Theta_2 &= {}^1\!/_2\Pi + {}^4\!/_3,\quad \Pi \to \infty. \end{aligned} \tag{14}$$

[34] Solutions (4) can be merged as follows:

$$\Theta(\Pi) = \frac{\Theta_1}{1 + \zeta\Pi^2} + \frac{\Theta_2\zeta\Pi^2}{1 + \zeta\Pi^2}. \tag{15}$$

[35] This approximation for $\zeta = 15$ does not deviate by more than 2% from the analytical solution (13) over the entire range of Π. Finally, the conduit friction force can be expressed as $F_\mu = 2\tau_w/r = 2\tau_b\Theta(\Pi)/r$. We note that a finite pressure gradient is necessary to initiate the flow in the case of Bingham liquid, in contrast to a Newtonian liquid.

[36] As from *Melnik and Sparks* [2002] we assume that viscosity of the magma is a product of the viscosity of pure melt $\mu_m(c, T)$ and a coefficient that represents the influence of the crystals $\theta(\beta)$. Viscosity of the pure melt is calculated according to *Hess and Dingwell* [1996]. The coefficient $\theta(\beta)$ is calculated according to

$$\log(\theta(\beta)/\theta_0) = \arctan(\varepsilon(\beta - \beta_*)) + \pi/2. \tag{16}$$

[37] Values of the dimensionless coefficients of θ_0, ε and β_* are given in Table 1. The coefficients in equation 16 have a major influence on eruption dynamics but there is only limited experimental data on their values. Thus, in this study, they are kept constant at values consistent with

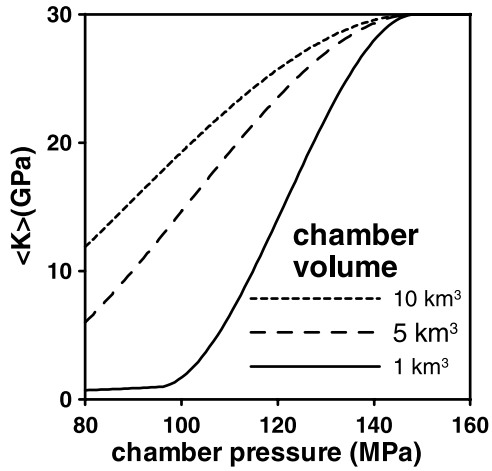

Figure 3. Bulk modulus of the magma inside the chamber as a function of the pressure at the top of the chamber for the top of the chamber located at 5 km depth and initial water content equal to 5 wt%. At low chamber pressures, bubble concentration inside the chamber is high, leading to low bulk modulus. As the chamber pressure increases, the bubble fraction in the chamber decreases, and the bulk modulus of the magma reaches the bulk modulus of pure melt (30 GPa in this study).

empirical calibration based on observations of the Soufrière Hills lava dome extrusion dynamics [*Melnik and Sparks*, 2002].

2.4. Boundary Conditions

[38] Equations (1a)–(1f) are solved numerically between the top of the magma chamber and the top of the lava dome. Flow in the dome is represented by a continuation of the conduit, with the same diameter for the active zone of flow within the dome and extrusion of new lava at the summit, consistent with observations [*Young et al.*, 1998, *Watts et al.*, 2002] for the Soufrière Hills Volcano. As the extrusion rate is subsonic, we assume that the pressure on the top of the dome is equal to atmospheric.

[39] We assume that the magma chamber is located in elastic rocks and is fed from below with new magma. The relation between pressure at the top of the magma chamber p_{ch} (referenced hereafter as the "chamber pressure") and intensity of influx Q_{in} and outflux Q_{out} of magma from the chamber is given by [*Woods and Koyaguchi*, 1994; *Melnik*, 2000; *Barmin et al.*, 2002]:

$$\frac{dp_{ch}}{dt} = \frac{4E\langle K\rangle}{\langle\rho\rangle V_{ch}(3\langle K\rangle + 4E)}(Q_{in} - Q_{out}). \tag{17}$$

[40] Here V_{ch} is the volume of the magma chamber, $\langle\rho\rangle$ and $\langle K\rangle$ are the average density and bulk modulus of the magma, respectively, and E is the elastic modulus of the surrounding rocks. The average compressibility of magma is controlled by the presence of bubbles and pressure distribution inside the chamber [*Huppert and Woods*, 2002]. Figure 3 shows the dependence of $\langle K\rangle$ on the pressure at the top of the chamber for a hydrostatic distribution of pressure for a spherical magma chamber located at depth of 5 km and having 5 wt% of dissolved water. When the pressure is low, a large part of the magma chamber is occupied by bubbly liquid and the average compressibility is high (i.e., $\langle K\rangle$ is low). When the pressure reaches the saturation pressure the entire chamber is filled by homogeneous magma and $\langle K\rangle$ increases strongly. For a larger magma chamber volume more of the chamber is occupied by homogeneous magma, therefore the average compressibility is smaller. Alternative assumptions on the geometry of the chamber will lead to some differences in the relationship between pressure and compressibility. Since chamber shape is poorly constrained in all field cases, we hereafter make calculations for spherical chambers.

[41] We also assume that the volume concentration of phenocrysts and mass transfer between the melt and bubbles in the magma chamber are in equilibrium. Thus we do not consider crystallization kinetics inside the chamber as developed in the model of *Bonnefoi et al.* [1995, 1999]. In these models it is proposed that rapid (nonequilibrium) crystallization can occur as a result of cooling of magma inside the chamber. Development of large undercoolings, however, are difficult to achieve for slow changes in pressure-temperature conditions. In our model the volume fraction of microlites is assumed to be zero at the conduit entrance because the large undercoolings that are required for crystal nucleation are unlikely to develop. Magma and gas velocities are equal, assuming the magma is impermeable at the low volume fraction of bubbles.

3. Numerical Method

[42] The integration interval $x \subseteq [0,L]$ is divided by nonuniform mesh containing n points with the step of the mesh decreasing toward the top of the conduit where gradients of variables reaches their maximum. System (1) can be represented as $\mathbf{F}(\mathbf{U}_{j-1},\mathbf{U}_j) = 0$, where $\mathbf{U}_j$ is vector function, represents dependent variables on jth interval of the mesh. By taking the first member of Taylor series, we obtain

$$0 = \mathbf{F}(\mathbf{U}_{j-1},\mathbf{U}_j) = \mathbf{F}(\mathbf{U}^*_{j-1},\mathbf{U}^*_j) + \left.\frac{\partial\mathbf{F}}{\partial\mathbf{U}}\right|_{\mathbf{U}^*_{j-1}}\Delta\mathbf{U}_{j-1} + \left.\frac{\partial\mathbf{F}}{\partial\mathbf{U}}\right|_{\mathbf{U}^*_j}\Delta\mathbf{U}_j. \tag{18}$$

[43] Here the asterisk symbol is a value of the function on the previous iteration, and $\Delta\mathbf{U}$ is the increment. Solving (18) in respect to $\Delta\mathbf{U}_j$ leads to the following matrix equation.

$$\Delta\mathbf{U}_j - \mathbf{P}_j\Delta\mathbf{U}_{j-1} = \mathbf{Q}_j;\ \mathbf{P} = \left.\frac{\partial\mathbf{F}}{\partial\mathbf{U}}\right|_{\mathbf{U}^*_{j-1}} \bullet \left(\left.\frac{\partial\mathbf{F}}{\partial\mathbf{U}}\right|_{\mathbf{U}^*_j}\right)^{-1};$$
$$Q = \mathbf{F}(\mathbf{U}^*_{j-1},\mathbf{U}^*_j) \bullet \left(\left.\frac{\partial\mathbf{F}}{\partial\mathbf{U}}\right|_{\mathbf{U}^*_j}\right)^{-1} \tag{19}$$

[44] System (19) is solved by means of the two-point chaser method as shown below:

$$\Delta\mathbf{U}_n = \mathbf{P}_n\Delta\mathbf{U}_{n-1} + Q_n = \mathbf{P}_n(\mathbf{P}_{n-1}\Delta\mathbf{U}_{n-2} + \mathbf{Q}_{n-1}) + \mathbf{Q}_n = \ldots = \mathbf{\Psi}_2\Delta\mathbf{U}_1 + \Theta_2. \tag{20}$$

[45] First we calculate matrixes Ψ and $\mathbf{\Theta}$ and with the help of boundary conditions $\boldsymbol{\varphi}\Delta\mathbf{U}_n + \boldsymbol{\theta} = 0$ find the values

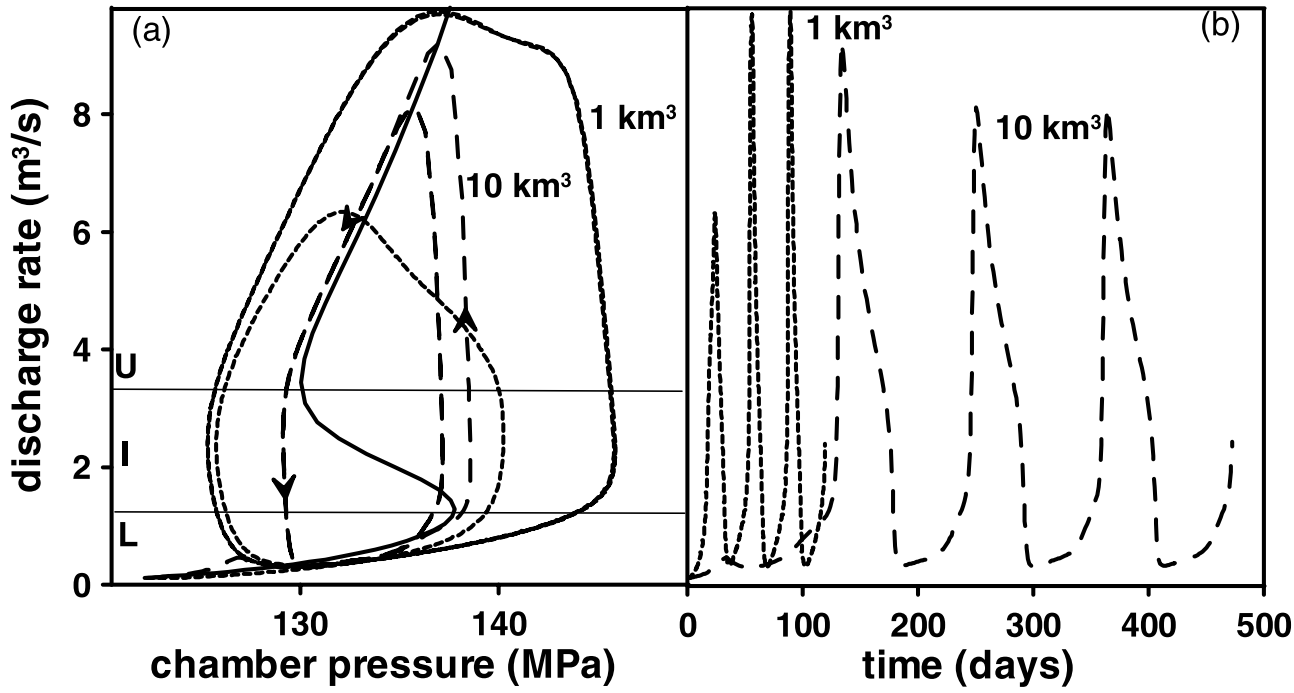

Figure 4. Calculations for the basic set of parameters (Table 1), except for chamber volumes. Dependence of discharge rate (a) on chamber pressure and (b) on time for the chamber volume of 1 (short-dashed line) and 10 (long-dashed line) km^3. Steady state solution is shown in Figure 4a (solid line). For chamber volumes greater than 10 km^3 the system shows quasi-static behavior. Here and after "chamber pressure" means pressure at the top of the magma chamber (bottom of the conduit).

of $\Delta \mathbf{U}_1$. Later, using equation (19), the calculation of all flow parameters is performed on a new iteration. Solution on a new time step is considered to be converged if the sum of $\Delta \mathbf{U}_i^2$ is smaller than a given value.

4. Results of Numerical Simulations

4.1. Basic Set of Parameters

[46] We will study the influence of controlling parameters on magma flow dynamics in the conduit by comparing calculations made with a basic set of parameters. We chose the "basic" parameters based on previous studies of the Soufrière Hills Volcano, Montserrat [*Melnik and Sparks*, 1999, 2002]. The choice of this particular set of parameters is somewhat arbitrary, but serves as a datum for considering how variations in parameters might affect model outputs. The values and ranges of the basic parameters are listed in Table 1, and the plots of discharge rate as a function of chamber pressure and time for the basic set of parameters are shown in Figure 4. For a magma chamber with a top located at 5 km depth the lithostatic pressure is calculated at 127 MPa for an average rock density of 2600 kg m^{-3}. Thus, for our basic parameters magma with 5 wt% of water in the melt phase will be supersaturated at lithostatic chamber pressure. Although the lithostatic pressure does not enter the problem directly, the chamber pressure cannot be significantly different from the lithostatic pressure. Overpressures above lithostatic pressure are unlikely to be greater than the strength of the chamber wall rocks, for example. Consideration of these limitations on realistic chamber pressures become important in the interpretation of the numerical results.

[47] As shown previously [*Melnik and Sparks*, 1999; *Barmin et al.*, 2002; *Melnik and Sparks*, 2002] the steady state solution of a boundary value problem may not be unique; for certain fixed parameters in the magma chamber, there could be up to three steady state regimes of extrusion. The uppermost regime is characterized by high discharge rate and either no or low rates of crystallization, so that conduit resistance is controlled by a relatively low magma viscosity, allowing high ascent velocity. In the lowermost regime, crystallization during magma ascent is significant, and conduit friction is high due to the relatively high viscosity of magma in comparison with the magma that failed to crystallize during ascent. In the intermediate regime, conduit resistance decreases with increase in discharge rate due to the decrease in crystal content and, therefore, the relative viscosity of the magma. Calculations based on the simplified transient model [*Barmin et al.*, 2002] indicate that the intermediate regime for a wide range of parameters is unstable.

[48] The asymptotic behavior for $t \rightarrow \infty$ of the transient solution depends on the value of Q_{in}. If Q_{in} corresponds to the upper (marked as "U" in Figure 4a) or the lower ("L") regime the discharge rate will stabilize with time with $Q = Q_{in}$. However, if Q_{in} corresponds to the intermediate regime ("I"), periodic variation in the discharge rate can occur. Here we compare magma chamber volumes of 1 and 10 km^3, with the influx corresponding to the intermediate regime. For V_{ch} = 10 km^3 the system behaves quasi-statically: the eruption starts within the regime with low

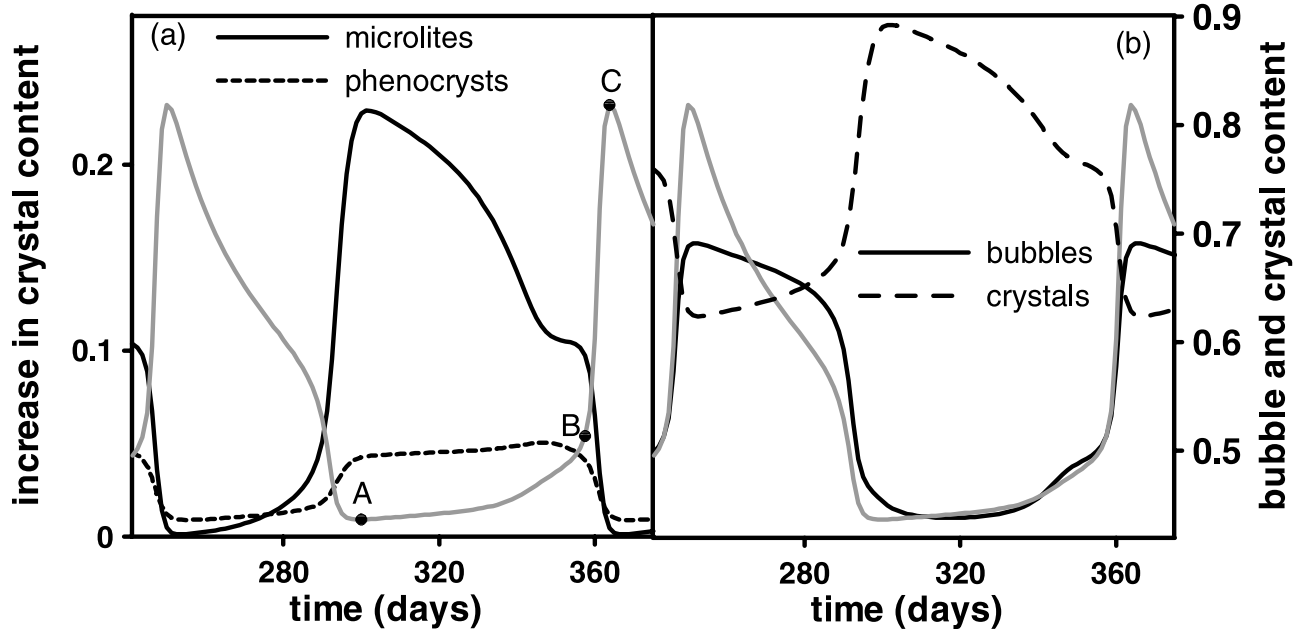

Figure 5. Variation of crystal and bubble content at the top of the conduit during one period of a cycle for the basic set of parameters and chamber volume of 10 km^3. The gray curve is a plot of discharge rate versus time identical to the calculation shown in Figure 4b for V_{ch} = 10 km^3. For reference purposes discharge rates at points A, B, and C are 0.32, 1.9, and 8.1 m^{3}s^{-1}, respectively.

discharge rate, closely following it up to the transition point, and then jumps to the uppermost regime. The eruption then follows the uppermost regime until the second transition point and jumps down to the lowermost regime. The transition between the regimes occurs with nearly constant chamber pressure. This behavior leads to periodic variations in discharge rate with time (Figure 4b).

[49] For V_{ch} = 1 km^3 the system starts in the lower regime and progressively departs from the steady state solution, reaching a slightly higher chamber pressure in the first cycle, moves to high discharge rates and lower chamber pressure, and then the discharge rate decreases significantly. The second and further cycles are nearly identical and the amplitudes of pressure and discharge rate variations are larger in comparison with the case for V_{ch} = 10 km^3 (Figure 4a). The eruption stabilizes with $Q = Q_{in}$ only in the case of unrealistically small magma chambers ($V_{ch} < 10^{-3}$ km^3). This result is in contradiction with *Barmin et al.* [2002] where the stabilization of the eruption occurred for large chamber sizes. This new result occurs because of much larger compressibility of the magma chamber due to the presence of bubbles, whereas as shown by *Barmin et al.* [2002], changes of the volume of the magma chamber occur only due to the elasticity of the surrounding rocks.

[50] Figure 5a shows the increase in crystal content due to crystallization inside the conduit ($\beta_{top} - \beta_{ch}$) for microlites (solid) and phenocrysts (dashed line). Figure 5b shows variations of total crystal and bubble content at the top of the conduit during one cycle for the basic set of parameters and V_{ch} = 10 km^3. As a reference discharge rate variation is plotted by gray line identical to Figure 4b. The calculations show that microlite crystallization dominates during periods of low discharge rate, whereas the overgrowth of phenocryst rims becomes dominant during periods of high discharge rate. Overall increase in crystal content can reach up to 25% for slowly ascending magma and only a few percent at high ascent rates. Rapid variations in discharge rate during transitions between the low and upper regimes are marked by rapid changes in crystal content. Total crystal content may reach up to 90% of condensed phase (Figure 5b). Changes in bubble content are due to a combined effects of gas exsolution and escape by permeable flow through ascending magma. Because gas escape is a slow process during a period of high discharge rate gas volume fraction increases up to 70% and decreases below 45% for low discharge rates. Calculated volume fractions of bubbles are generally higher than observed during lava dome building eruptions. The model underestimates near-surface degassing because it assumes only vertical gas flux. However, in the volcanic edifices and in the domes itself significant gas escape can occur laterally. High bubble content at high discharge rates may lead to the transition to explosive eruption if, for example, lava dome collapse occurs.

[51] Figure 6 shows distributions of different parameters along the conduit for three discharge rates marked in Figure 5a: A is minimum; B is intermediate, and C is maximum discharge rate during the cycle. Rapid increase in crystal content at low discharge rate (A) occurs at a depth of 2.5 km (Figure 6a), when due to increase in undercooling (Figure 6d), rapid nucleation of microlites occurs (Figure 6f). At greater depths crystallization occurs only by the growth of existing phenocrysts (Figure 6e). Because of rapid crystal growth, undercooling decreases, and as a consequence, nucleation of microlites stops at a depth of 2 km. At shallower depths crystal growth occurs on existing crystals. At a depth of 200 m a second nucleation event occurs when magma is strongly degassed. Two nucleation events calculated for low discharge rates will result in

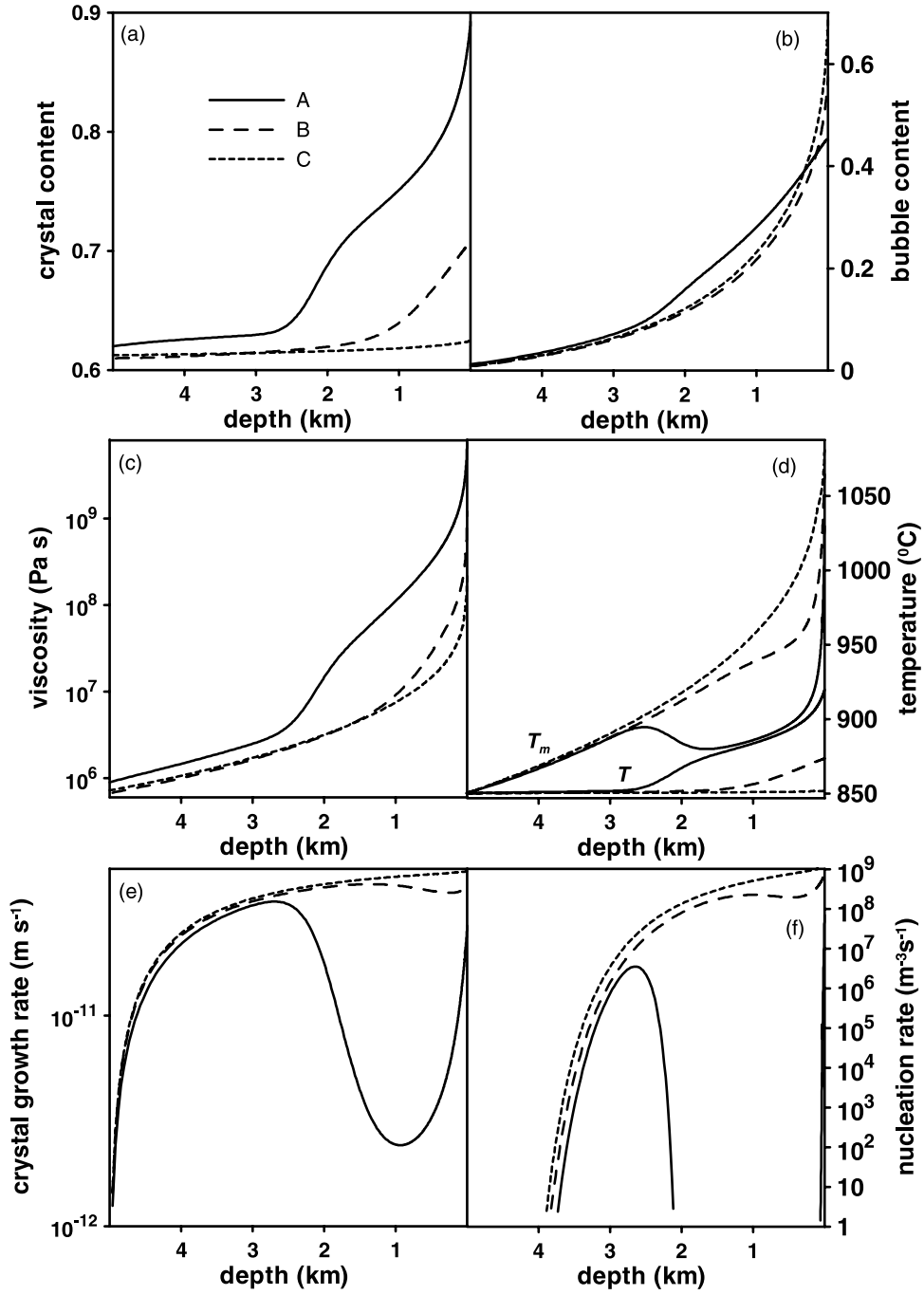

Figure 6. Profiles of parameters along the conduit for three different discharge rates marked in Figure 5a: (a) crystal content, (b) volume fraction of bubbles, (c) viscosity, (d) magma temperature (T) and effective melting temperature (T_m, see equation (9)), (e) crystal growth rate, and (f) nucleation rate for microlites. Solid curves (A) correspond to minimum discharge rate; long-dashed curves (B) correspond to intermediate discharge rate, and short-dashed curves (C) correspond to maximum discharge rate as labeled in Figure 5a. The difference between T_m and T is undercooling.

bimodal crystal size distribution of groundmass crystals. Rapid crystallization leads to oversaturation of the remaining melt, intense diffusion of volatiles and growth of bubbles (Figure 6b). However, permeability development and gas escape counteracts these processes. Because of crystal growth, viscosity increases rapidly (Figure 6c) and at the top of the conduit is 2 orders of magnitude higher compared to the case (C) at high discharge rate. The release of latent heat of crystallization leads to increase in magma temperature at the top of the conduit up to 60°C in comparison with initial temperature (Figure 6d).

[52] In the case of maximum discharge rate (C) undercooling increases monotonically leading to monotonic increase in both crystal growth and nucleation rates. Although

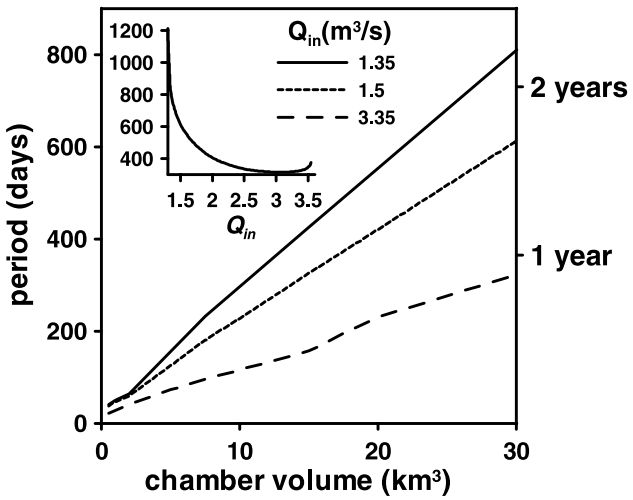

Figure 7. Period of oscillations in discharge rate as a function of chamber volume V_{ch} for the three values of the influx into the chamber Q_{in}. The dependence of the period (in days) on influx for V_{ch} is shown in the frame.

these rates are higher than for the case of low discharge rate (A) the much shorter transit time through the conduit leads to overall lower crystal content than in the case (A). Case (B) shows intermediate behavior.

[53] General trends predicted by the model agree with observations on several lava dome building eruptions. On Mount Unzen and the Soufrière Hills Volcano good correlation between discharge rate and porosity of magma and anticorrelation between discharge rate and its crystallinity has been inferred [*Nakada et al.*, 1999; *Sparks et al.*, 2000]. Our model provides a framework for interpreting textures in lava dome samples and interpretation of crystal size distributions (CSD). We stress that the calculations shown in Figures 5 and 6 are for particular sets of parameters. The modeling parameters would need to be modified for individual magma systems to compare model predictions with specific textural observations.

[54] The period of oscillations in discharge rate is a function of magma chamber size, magma compressibility inside the chamber, and intensity of magma recharge and evacuation (Q_{in} and Q_{out}, see equation 6). Figure 7 shows the influence of Q_{in} and magma chamber size on the period when Q_{in} corresponds to the unstable branch of the solution and undamped oscillations are possible. There is a minimum of the period that corresponds to Q_{in} in the middle between transition points to the upper and the lower regimes (see the inset in Figure 7). When Q_{in} is close to one of the transition points, the rate of pressure change in the magma chamber $\sim Q - Q_{in}$ is low, and therefore the time that the system spends near the transition points increases. This leads to the increase in the period. The general trend of the calculated period is in a good agreement with the equations derived by *Barmin et al.* [2002], although the shape of the curves are slightly different.

4.2. Influence of the Initial Phenocryst Size

[55] As we assume that all phenocrysts, assumed spherical, are already present in the magma chamber and have the same radii R_{ph}, the total phenocryst surface area S_{ph} is inversely proportional to the phenocryst radii ($S_{ph} = 4\pi R_{ph}^2 N_{ph} = 3\beta_{ph}/R_{ph}$). Therefore, for the same volume fraction of crystals, the surface area and, subsequently, the mass transfer rate to crystals will be higher for a magma with smaller crystal sizes. We assume that there

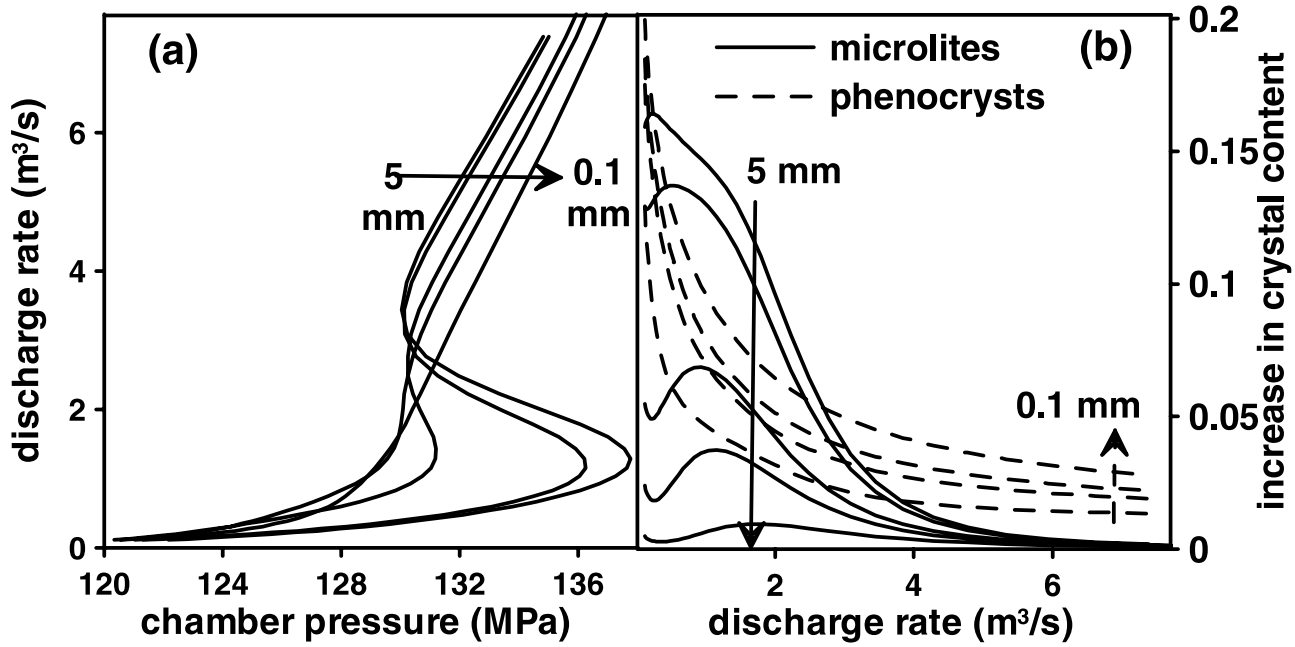

Figure 8. Influence of the initial phenocryst size on eruption dynamics. (a) Steady state solutions (discharge rate versus chamber pressure) for phenocryst sizes 0.1, 0.75, 1, 2.5, and 5 mm. (b) Variation of the phenocryst and microlite contents with discharge rate along the corresponding steady state solutions. Arrows show the directions of decrease in phenocryst sizes for corresponding curves.

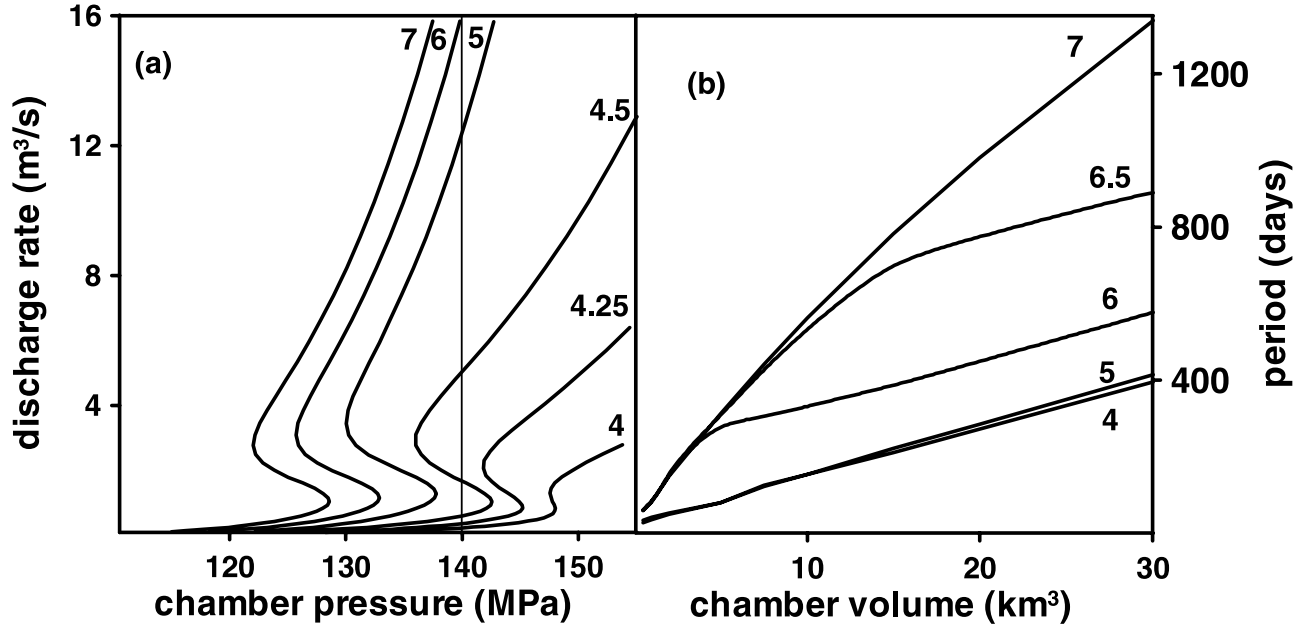

Figure 9. (a) Steady state solutions for different initial water contents c_0 (marked on the curves, in wt%). (b) The period of oscillations in discharge rate as a function of chamber pressure for different values of c_0. For high water content, magma chamber contains gas in bubbles and has low bulk modulus resulting in longer periods of pulsations.

are no microlites inside the chamber, and initial concentration of phenocrysts is assumed to be equilibrium (see equation 8).

[56] Figure 8 shows calculations of the relationship between discharge rate, chamber pressure and crystal content. In Figure 8a the variation of discharge rate with chamber pressure is shown for various phenocryst size with radii from 0.1 to 5 mm. In Figure 8b the amount of crystal growth during ascent in the conduit is shown as a function of discharge rate for the same cases as in Figure 8a with variable initial phenocryst sizes. The proportions of growth of the existing phenocrysts and microlites are distinguished. In the case of small phenocrysts (0.1 mm) their surface is sufficiently large so that nearly all crystal growth occurs on existing crystals, and the microlite content is less than 1% (see Figure 8b). The variation of the crystal content with discharge rate in this case is smaller than for the cases with significant microlite growth, and therefore the viscosity variations associated with crystallization are smaller. As a consequence, the dependence of discharge rate on chamber pressure is monotonic and periodic behavior does not occur.

[57] As phenocryst size increases and surface area per unit volume decreases their contribution to crystallization during ascent is reduced. Large magma undercoolings are reached resulting in microlite nucleation and growth. The characteristic sigmoidal curve for discharge rate versus chamber pressure appears for phenocryst size of 0.75 mm or greater; for these conditions periodic behavior becomes possible. Microlite content has a maximum in discharge rate because at lower discharge rate more undercooling is removed by the growth of the phenocrysts, whereas at higher discharge rates overall time for crystal growth decreases leading to decrease in crystal content. These results show that eruptive behavior is expected to be sensitive to the mean phenocryst size and phenocryst size distribution in the magma chamber.

4.3. Influence of Total Concentration of Dissolved Gas on Ascent Dynamics

[58] Total concentration of dissolved gas c_0, assumed here to be water, can be constrained by petrological methods by analyzing melt inclusions [*Wallace et al.*, 1995]. Typical melt water contents are taken to be 4–7 wt% for lava dome eruptions. Total gas content and chamber pressure control the volume fraction of bubbles inside the magma chamber and, therefore, magma compressibility. For pressures less then the saturation pressure, according to the solubility law, there is a free gas phase in bubbles. As shown by *Huppert and Woods* [2002], the presence of bubbles in the magma chamber can increase the duration of the eruption and the volume of erupted material by up to two orders of magnitude compared to the case of bubble-free magma.

[59] Steady state solutions are shown in Figure 9a. With increase in c_0 the average density of magma inside the conduit decreases and, therefore a lower chamber pressure is required for the same discharge rate. The discharge rates at the transition points only slightly depend on c_0 if the magma is supersaturated in the chamber. For low values of c_0 (<4.5 wt%) the magma in the conduit is initially undersaturated and remains as an homogeneous liquid for a large vertical part of the conduit. This means that decompression-induced crystallization occurs only at the upper part of the conduit and variations in crystal content with discharge rate are small. Therefore the interval of discharge rates where oscillatory behavior is possible shrinks as c_0 decreases.

[60] The numerical results are usefully considered in the context of the likely values of lithostatic pressure and limits

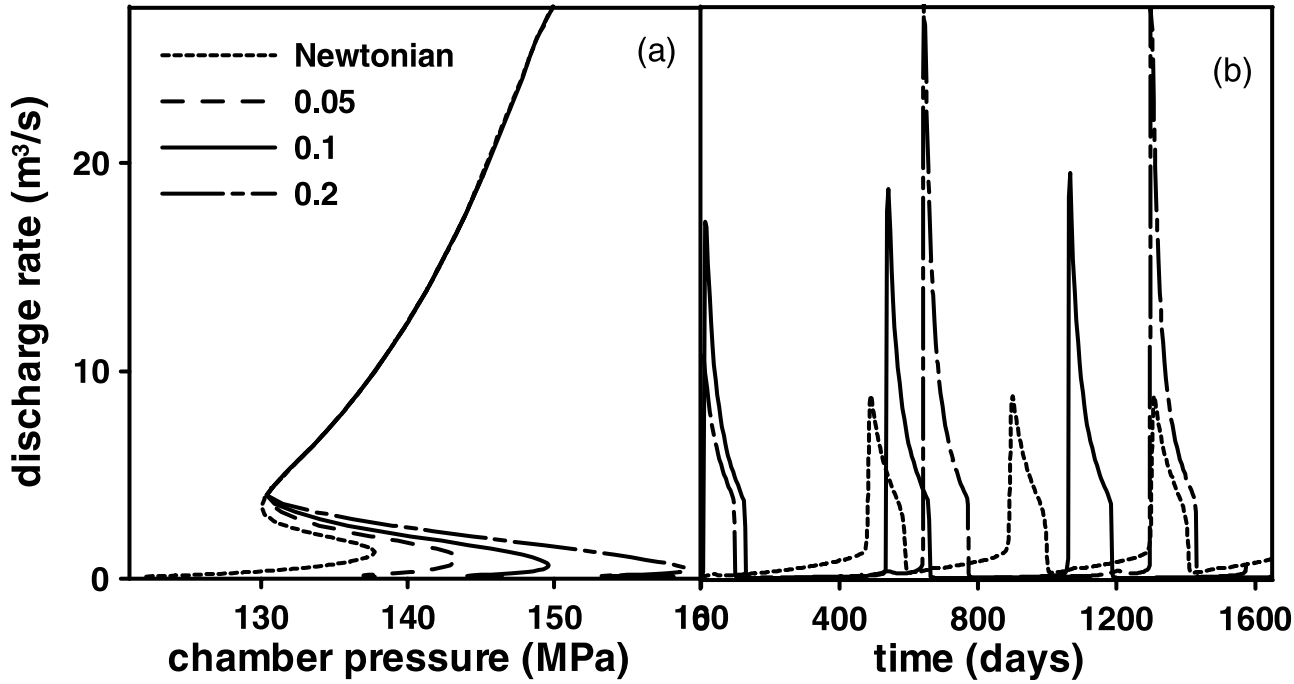

Figure 10. Steady state solutions and dependence of discharge rate on time for Newtonian and Bingham rheology of the magma. Yield strength is a parameter marked on the curves (values in MPa). For Bingham rheology discharge rate remains zero between the pulses of activity. Bingham rheology results in much higher chamber pressures prior to the onset of activity and, therefore, much higher discharge rates in comparison with Newtonian rheology.

on chamber overpressures due to chamber wall strength. For L = 5 km we take 127 MPa as a lithostatic pressure and 140 MPa as a representative upper limit on overpressure for illustration (thin line in Figure 9a). Solutions for c_0 < 4.25 wt% require chamber overpressures that are unrealistically high. The sensitivity of the dynamic conditions to water content can be illustrated by comparing the case of 4.5 and 5 wt% at a chamber pressure of 140 MPa. At c_0 = 4.5 wt% the system is calculated to be in the oscillatory regime for Q_{in} = 2 m^3 s^{-1} with discharge rate pulses reaching 5 m^3 s^{-1} in the upper regime. If the water content increases up to 5 wt% (for example by influx of new gas related to chamber replenishment) the system will move to an upper regime with a discharge rate of 12.5 m^3 s^{-1}. Thus small changes in volatile content can result in large changes in discharge rate. Further, for the example considered, 12.5 m^3 s^{-1} may be sufficiently high that conditions for explosive eruption might then develop, based on empirical evidence that explosive activity commonly develops in dome eruptions when $Q_{out} \geq$ 10 m^3 s^{-1} [*Jaupart and Allegre*, 1991; *Woods and Koyaguchi*, 1994].

[61] Figure 9b shows the period of oscillations as a function of chamber volume and water content. For c_0 = 4.5 and 5 wt% the volume fraction of bubbles in the chamber is very small so that mixture compressibility is low and is determined by the compressibility of pure magma. Therefore the period of pulsation is small and linearly depends on the chamber size. For c_0 = 7 wt% the volume fraction of bubbles is significant for all magma chamber volumes leading to high magma compressibility and long periods. In the case c_0 = 6 and 6.5 wt% for a small magma chamber the compressibility is high and the period is longer than for c_0 = 5 wt%. With increase in the chamber size the proportion of the chamber occupied by bubbly magma and average compressibility decreases and the period of pulsation is much smaller than for c_0 = 7 wt%. The accuracy of the model decreases for small chamber sizes and high water contents when volume fraction of the bubbles inside the chamber is sufficiently high. This is due to the fact that a hydrostatic pressure distribution inside the chamber is calculated based on the density of magma without bubbles assuming that the volume fraction of bubbles is small. This pressure distribution is used for calculations of the average compressibility of the magma $\langle K \rangle$ in equation (17). Therefore the model underestimates magma compressibility and the resulting periods are shorter than they should be if accurate account had been taken for the pressure distribution inside the chamber.

4.4. Influence of Non-Newtonian Properties on Eruption Behavior

[62] Now we compare the dynamics of magma extrusion in the cases of Newtonian and Bingham rheology. We will assume that yield strength appears when the concentration of crystals reaches a critical value:

$$\tau = \begin{cases} \tau_b \text{ for } \beta > \beta_{cr} \\ 0 \quad \text{for } \beta \leq \beta_{cr} \end{cases}. \tag{21}$$

[63] Figure 10a shows a set of steady state solutions for different values of τ_b. Values of τ_b and β_{cr} depend on crystal

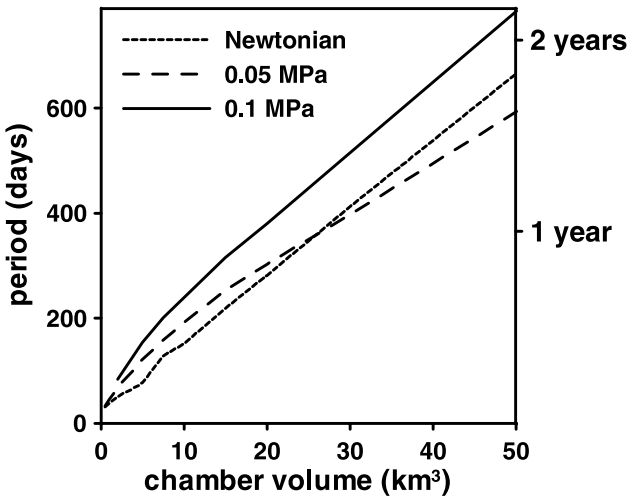

Figure 11. Comparison of the period of pulsation in discharge rate for Newtonian and Bingham rheologies.

shape, crystal size distribution, magma temperature and other properties. To illustrate the influence of Bingham rheology the value of $\beta_{cr} = 0.65$ was chosen so that for the uppermost regime, the magma has Newtonian rheology. A more detailed study would require measurements of the rheological properties of magma at a wide range of crystal content and crystal size distribution. The higher the value of τ_b the larger the chamber pressure that is necessary to start the eruption. Initial chamber overpressure (above hydrostatic) can be estimated as

$$\Delta p_{init} = \frac{4}{D}\int_o^L \tau(\beta(x))dx = \frac{4}{D}\tau_b(L - L_b), \qquad (22)$$

where $\beta(x)$ represents the distribution of crystal content along the conduit, L_b is the position in the conduit (measured from the bottom) where β_{cr} is reached. If the chamber overpressure is lower then Δp_{init} the eruption is not possible. For $\tau_b = 0.1$ MPa and $L_b \sim 2600$ m (taken from the steady state solution with low discharge rate (5×10^{-4} m^3 s^{-1}) the value of Δp_{init} is 32 MPa, for example.

[64] Figure 10b shows the influence of these two rheological models on the dynamics of magma extrusion. In the case of Bingham rheology discharge rate between the two pulses is zero until the critical chamber overpressure is reached. Then the discharge rate increases rapidly with decrease in crystal content, leading to a significant reduction of both magma viscosity and shear force associated with yield strength proportional to $(L - L_b)$. The system transits to the uppermost flow regime and the pressure then decreases quickly. Because the pressure on the onset of the pulse was significantly larger then in the case of a Newtonian liquid the resulting discharge rate in the case of Bingham rheology is also significantly higher.

[65] Due to the limitations of the current transient numerical code, the minimum discharge rate is limited to about $Q_{\min} = 10^{-2}$ m^3 s^{-1}, therefore, truly zero discharge rates are not attained in the model. Particular values of minimum discharge rates play a minor role in the eruption dynamics if the chosen value is much smaller than the value of Q_{in}, because the values of $Q_{\min}$ and Q_{in} control the evolution of the pressure inside the magma chamber during a period of no or little discharge from the conduit.

[66] The period of pulsation (Figure 11) in the case of a Bingham rheology may be either longer or shorter than in the case of Newtonian rheology. This result is due to the counteracting effects of two processes: for Bingham rheology the chamber pressure has to reach much higher values before the next pulse of activity occurs, but at the same time the pressure inside the magma chamber grows faster because there is no outflux of the magma from the chamber between the pulses. The calculated timescales of months to several years are consistent with observations. In all the calculated cases the difference in the periods is less than a factor of 1.5 times for fixed magma chamber volumes in the range of 0.5 to 50 km^3.

[67] Because of the change of the topology of the steady state solution (Figure 10a) there is a much wider interval of discharge rates corresponding to periodic behavior. For the chosen set of parameters, periodic behavior occurs for $Q_{in} > 0.5$ m^3 s^{-1} for the Bingham rheology with $\tau_0 = 0.1$ MPa and $Q_{in} > 1.32$ m^3 s^{-1} for the Newtonian case. The period between the pulses increases inversely with decrease in Q_{in}, leading to periods of 1.41, 2.58 and 7.25 years for $Q_{in} = 2$, 1 and 0.5 m^3 s^{-1} for $V_{ch} = 30$ km^3 and $\tau_0 = 0.1$ MPa.

[68] It is instructive again to consider realistic values of chamber pressure. In Figure 10a chamber pressures, for large values of τ_0, have to reach values which are greatly in excess of lithostatic pressure at 5 km. The high overpressures needed to initiate flow may thus never be realized. However, the response of the system may be to widen the conduit, a process that is not considered here since the calculations assume a cylindrical conduit with constant diameter.

4.5. Influence of Initial Magma Temperature and Conduit Diameter

[69] Both magma temperature and conduit diameter have a strong influence on discharge rate. Decrease in temperature leads to increase in magma viscosity and decrease in crystal growth rate [*Hammer and Rutherford*, 2002; *Couch et al.*, 2003]. The values of discharge rate at the transitional points decrease slightly as temperature decreases as a consequence of decrease in crystal growth rate (Figure 12a), whereas the values of chamber pressure at transition points are significantly larger for low temperatures, because of increasing magma viscosity. Consider a representative chamber pressure of 135 MPa (thin line in Figure 12a). At 850°C there are two stable steady solutions so that periodic behavior can take place in response to magma chamber replenishment with relevant Q_{in} and chamber pressure variations between the transition points. If the chamber cools to 825°C flow can only occur in the lower regime (at 135 MPa) at negligibly slow rates. If the chamber heats up to 875°C the flow rate will increase to very high values in the upper regime, and indeed will be so high that explosive eruption might be expected.

[70] For the Newtonian incompressible liquid with constant viscosity discharge rate is proportional to D^4. Therefore small changes in conduit diameter will lead to large changes in discharge rate. Magma ascent velocity is pro-

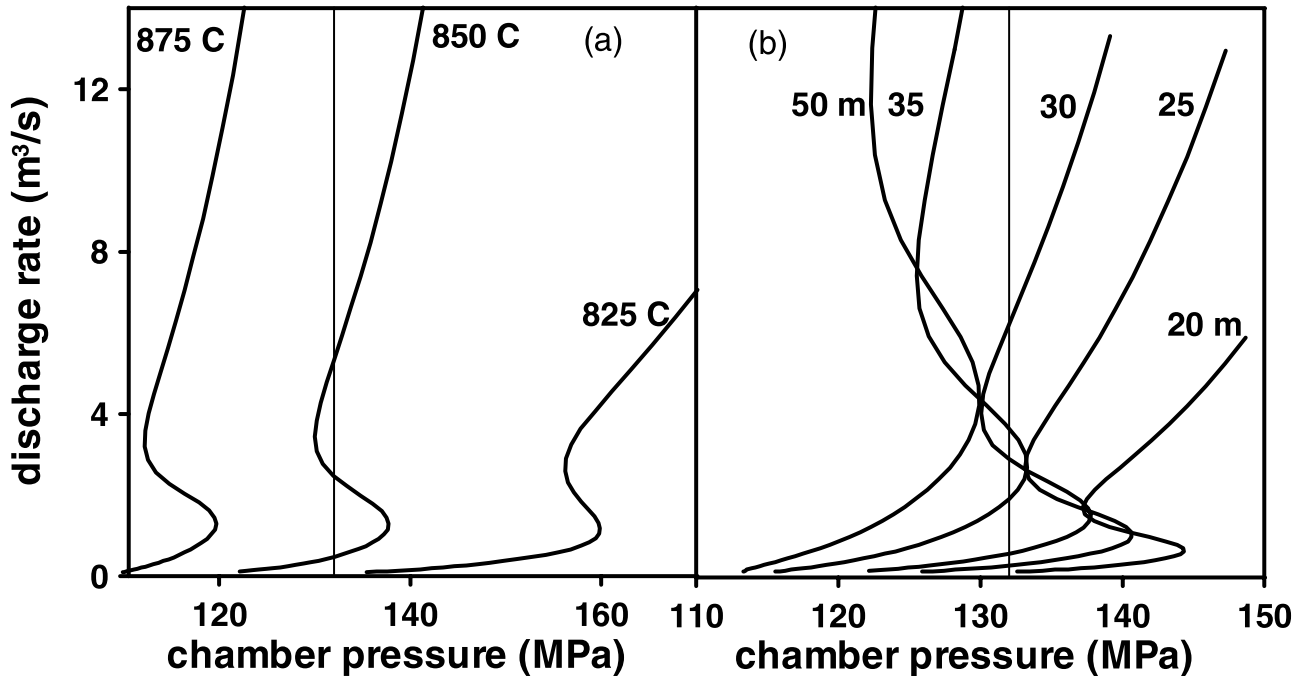

Figure 12. Steady state solution corresponding to different initial temperatures (in Celsius in Figure 12a) and different conduit diameters (in meters in Figure 12b).

portional to D^2 only. Therefore, for the same discharge rate crystallization will be more efficient in the wider conduit and the transition to the upper regime will occur at higher discharge rates (Figure 12b). Because of the sigmoidal shape of steady state solutions, small variations in conduit diameter can lead to significant changes in discharge rate. The sensitivity can be demonstrated by considering a fixed pressure of 132 MPa (thin line in Figure 12b). For d = 30 m the discharge rate at the upper stable regime is about 6 m^3 s^{-1}, but if the conduit narrows to d = 25 m (for example due to heat loss and magma crystallization on the conduit walls) the discharge rate drops to very small values ($\sim$0.25 m^3 s^{-1}).

4.6. Eruption Through the System of Interconnected Magma Chambers

[71] Until now we have considered that the influx into the magma chamber is constant throughout the eruption. Real magmatic systems can show more complicated behavior. Indeed magma supply systems are poorly constrained by observations, but the situation that there is a shallow peripheral magma chamber connected to a deeper magmatic chamber has been commonly accepted [e.g., *Murphy et al.*, 2000]. We will consider that eruption develops through a system of two magma chambers connected with each other with a conduit. For example, a system can be envisaged of a lower crustal deep chamber supplied by magmas from the underlying mantle which feeds magma into a shallow upper crustal chamber. The deeper chamber can be initially pressurized and prior to the eruption and has no influx of fresh magma from below. Alternatively, the deeper chamber can be fed by a constant or variable influx Q_{in}^d and initially have no overpressure. Alternative scenarios are also plausible. The variation of the chamber pressure in the deeper chamber will be controlled by deformation of the wall rocks and the intensities of magma supply and evacuation. Here we assume for illustration that the deformation is elastic:

$$\frac{dp_{ch}^d}{dt} = \frac{E}{V_{ch}^d}\left(Q_{in}^d - Q_{out}^d\right). \tag{23}$$

[72] Here the superscript "d" refers to deeper chamber. Discharge rate from the deeper chamber Q_{out}^d is considered to be equal to the discharge into the upper magma chamber Q_{in} and can be calculated as

$$Q_{out}^d = Q_{in} = \frac{d_d^4}{128\mu_b}\left(p_{ch}^d - p_{ch}\right). \tag{24}$$

where d_d is the diameter of the deeper conduit that connects two chambers, and μ_b is the viscosity of the magma in this conduit (assumed to be basalt). If the two chambers are connected with a dyke the coefficient in (24) will be different. As a first approximation the cross-section area of the lower conduit is assumed to be constant.

[73] Figure 13 shows discharge rate as a function of shallow chamber pressure and with time for the two cases: the first case (Figures 13a and 13b) involves a constant supply into the deeper chamber with $Q_{in}^d = 7$ m^3 s^{-1}, and the second case (Figures 13c and 13d) involves the deeper chamber is pressurized but receives no further supply.

[74] In the first case, pressure initially increases in the deeper chamber leading to the replenishment of the upper chamber. Initially influx into the upper chamber corresponds to the lower branch of the steady state solution, which relates the pressure in the upper chamber with discharge rate, and the upper chamber pressure initially increases monotonically. The system follows the lower branch of the steady state solution. When Q_{in} reaches the

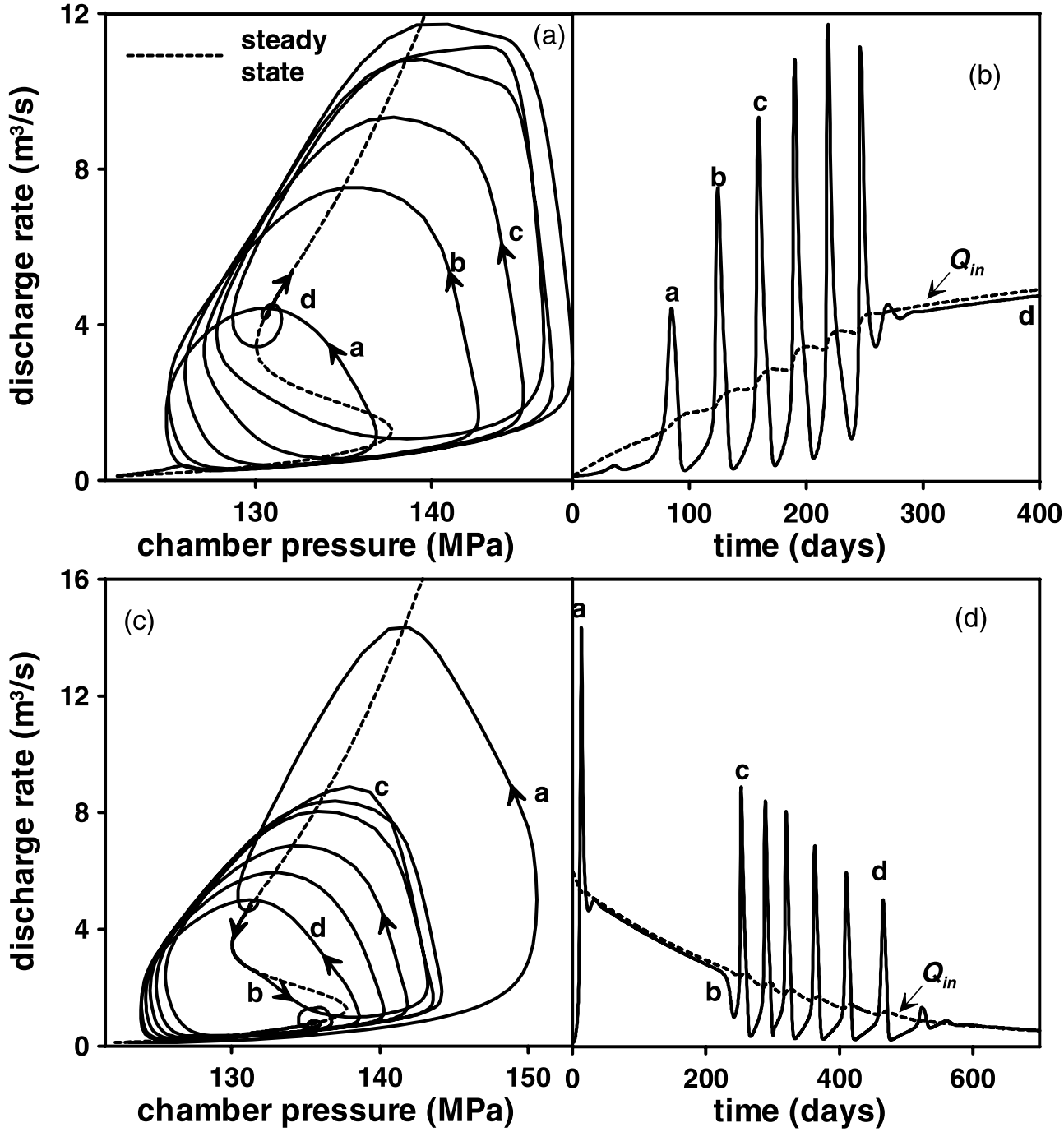

Figure 13. Phase diagrams and variation of discharge rate with time for eruption through a system of two interconnected chambers. The volume of the lower chamber is 10 km^3, and the upper chamber is 1 km^3. The lower chamber has a depth of 15 km and is connected with the upper chamber by a conduit of 2 m in diameter. The viscosity of the magma in the lower chamber (assumed basalt) is 10^3 Pa s. In the first case (Figures 13a and 13b) the lower chamber is fed with constant influx Q_{in}^{d} = 7 m^3 s^{-1}. In the second case the lower chamber is isolated but initially pressurized. Influx rate into the upper chamber Q_{in} is shown in Figures 13b and 13d as short-dashed lines.

lower transition point oscillations start. Oscillations stop when the influx rate into the upper chamber becomes larger than the discharge rate corresponding to the upper transition point. The system follows the upper branch of the steady state solution as influx into the upper chamber increases. Finally the system will reach a steady state with the discharge rate equal to Q_{in}^{d}. The period of oscillations monotonically decreases as the influx into the chamber increases and chamber pressure increases at a faster rate.

[75] In the second case, initially the influx into the upper chamber corresponds to the upper branch of the steady state solution. After an initial sharp increase in discharge rate the

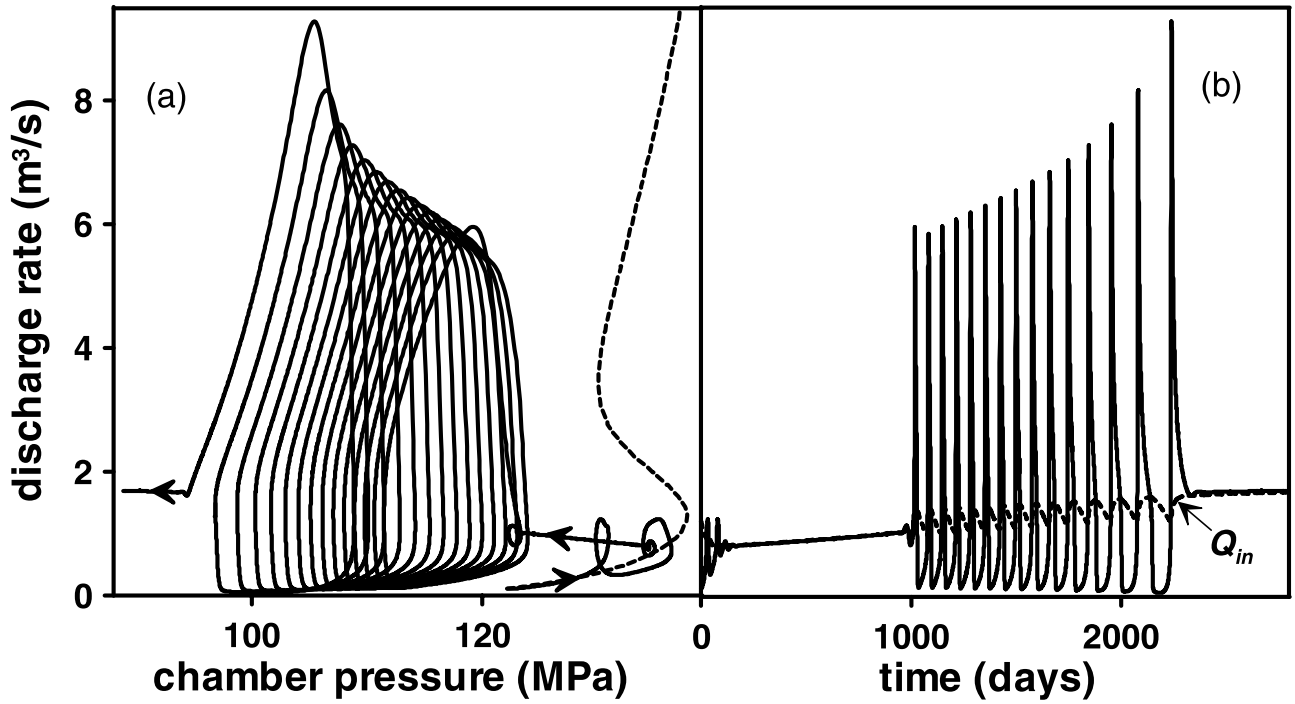

Figure 14. The same as Figures 13a and 13b, but the calculations take account of heat transfer between basalt and the magma in the upper chamber. Initial temperature of the basalt is 1100°C. The lower chamber has a volume of 500 km^3 and is initially pressurized.

system goes along the upper branch of the steady state solution as the pressure in the deeper chamber decreases resulting in the decrease in influx rate. After the influx to the upper chamber decreases to the upper transition point oscillations begin. Their period monotonically increases as Q_{in} decreases. Later with time the system stabilizes on the lower branch of the steady state solution and the intensity of the eruption decreases to zero.

[76] Changes from monotonic to periodic behavior are a common feature of extrusive eruptions. For example, on Mt. St. Helens (1980–1987) initial pulsatory dome growth was switched to steady growth for more than a year, and then was again altered to a pulse-like activity before stopping in 1986 [*Swanson and Holcomb*, 1990]. At the Soufrière Hills Volcano (Montserrat), short term pulses in extrusive activity with the period of 6 to 7 weeks were observed at a period of high dome extrusion rates [*Voight et al.*, 1999; *Sparks and Young*, 2002].

4.7. Temperature Variation Inside a Two-Layered Magma Chamber and Its Influence on Extrusion Dynamics

[77] Many dome-building eruptions appear to be associated with influx of the hot mafic magma into an open-system chamber. Examples include Mount Pinatubo [*Pallister et al.*, 1996] and Soufrière Hills, Montserrat [*Murphy et al.*, 2000]. Such open-system behavior can strongly affect eruptive dynamics. Here we present a simplified model to illustrate the kinds of complications that can occur. Because of the intrusion of hot basaltic magma into the bottom of the magma chamber, the temperature of the upper layer of evolved magma can rise with time [*Couch et al.*, 2001]. We modify the model suggested by *Huppert and Sparks* [1988] to account for the influx of the magma into the chamber. We neglect the processes of melting of the chamber walls and heat flux into the wall rocks because for a long-living magma chamber, thermal evolution of surrounding rocks is a slow process. The modified system of equations is

$$
\begin{aligned}
&m_b c_b \frac{dT_b}{dt} = Q_{in} c_b (T_{in} - T_b) - F_{bs} \\
&m_s c_s \frac{dT_s}{dt} = F_{bs} \\
&\frac{dm_b}{dt} = \rho_b Q_{in}; \quad \frac{dm_s}{dt} = -\rho_s Q_{out} \\
&F_{bs} = \Omega \rho_b c_b Y_b (T_b - T_{bs})^{4/3} = \Omega \rho_s c_s Y_s (T_i - T_{bs})^{4/3} \\
&Y_i = 0.1 \left(\gamma_i g k_i^2 / \nu_i\right)^{1/3}; \quad i = b, s.
\end{aligned} \tag{25}
$$

[78] Here index "i" = "b" corresponds to basaltic magma, "i" = "s" to silicic, m_i are masses of the layers, c_i are the specific heats, L_i are the latent heat of crystallization, F_{bs} is the heat flux due to the convective heat transfer, T_{bs} is the interface temperature, T_i are the temperatures of the layers, T_{in} is the temperature of influxing basaltic magma, Ω is the surface area of the interface between the magmas, γ_i are the thermal expansion coefficients, k_i are the thermal diffusivities, and ν_i are the kinematic viscosities of the layers, Y_i are the "intensity factors" [*Huppert and Sparks*, 1988]. We will assume that, initially, basalt occupies 10% of the volume of the chamber and has an average temperature of $(T_s + T_{in})/2$ and the influx Q_{in} is calculated based on equations (24, 25). The temperature of inflowing basalt T_b is assumed to be constant.

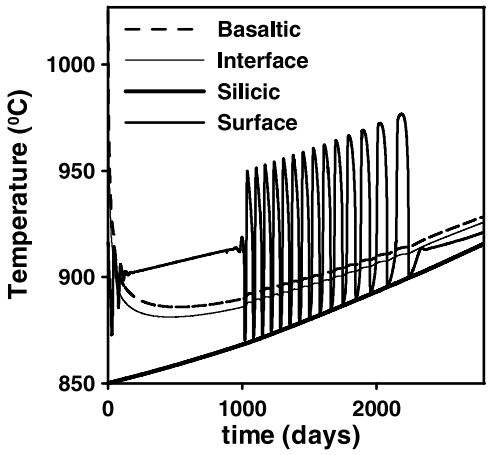

Figure 15. Variation of the temperatures inside the magma chamber (long-dashed line, basaltic layer; solid line, silicic; thin line, interface temperature between the layers) and at the top of the conduit (short-dashed line) with time. The initial temperature of basaltic layer is 1100°C; silicic layer has the temperature equal to 850°C. Because of the release of the latent heat of crystallization, the top-of-conduit temperature is higher that in the chamber. Peak values of surface temperature correspond to periods of low discharge rate when crystallization is significant.

[79] Figure 14 shows the evolution discharge rate at the top of the conduit as a function of chamber pressure at the upper chamber and time. The intensity of influx into the chamber is shown with the dashed line in Figure 14b. We assume that the lower chamber has a very large volume (500 km^3 for this calculation); therefore the pressure variation inside the deeper chamber is small. The deeper chamber is pressurized, corresponding to the initial intensity of influx equal to 1.2 m^3 s^{-1} which is lower than the discharge rate corresponding to the transition point on a steady state solution for the initial temperature (long-dashed line in Figure 14a). The eruption soon reaches a steady state regime with the influx to the upper chamber equal to the outflux through the conduit.

[80] As the temperature of silicic magma increases due to the influx of hot basalt (see Figure 15), the viscosity of the magma decreases and the upper chamber pressure also decreases (see Figure 12 a for the evolution of the steady state solution with temperature). Decrease in the pressure in the upper chamber leads to the increase in basalt influx into the chamber according to equation (24). Finally with both increase in influx rate into the upper chamber and changes in the steady state solution due to the changes in the upper chamber temperature, the system reaches unstable conditions and oscillations in discharge rate begin. The upper chamber pressure decreases progressively from one cycle to another because of the continues heating of the magma and influx rate increases too. Finally the system evolves to stable conditions again because influx rate corresponds to the upper branch of the steady state solution. Discharge rate continue to increase monotonically following increase in the influx rate.

[81] The temperature evolution inside the upper chamber and at the top of the conduit is shown in Figure 15. The temperature of the basaltic layer (dashed line) initially decreases rapidly because the volume of basalt is small and the temperature contrast is high. After ~500 days the temperature of the basaltic layer starts to increase because the volume of basalt increases due to the influx, and, the heat transfer to the silicic layer decreases because the temperatures of the two layers become closer. The temperature of silicic layer initially changes slower than the temperature of basaltic layer because of the larger volume initially occupied by silicic magma. Later the rates of temperature change become comparable as the proportion of the chamber occupied by basaltic magma increases. The surface (top-of-conduit) temperature initially stays higher than the chamber temperature, owing to the release of the latent heat of crystallization during magma ascent. The difference in the temperatures is about 60°C. Later, when oscillations in discharge rate begin, oscillatory variations occurs in the surface temperature. During periods of high discharge rate, when crystal growth is small, the change of the temperature inside the conduit also becomes small. During periods of low discharge rates, crystallization leads to the surface temperature increasing to high values.

5. Discussion

[82] We have developed a 1-D transient numerical model of the conduit flow in lava dome eruptions, which captures many of the principal factors that control discharge rate and eruptive style. Of particular importance is the kinetics of crystallization induced by magma degassing. Discharge rate is very sensitive to crystallization rate under certain conditions where the timescales of crystallization are comparable to magma ascent times. This arises because of the strong dependence of rheological properties on the crystal content, related to crystal-fluid interaction and latent heat effects. At high crystal contents crystal interactions and interlocking becomes particularly important [*Petford*, 2003].

[83] Three regimes are identified: (1) the flow rate is so fast that little crystallization occurs during ascent, and the magma is relatively low in viscosity; (2) the flow rate is sufficiently slow that extensive crystallization occurs and magma can erupt in a nearly solid state with very high viscosity and a yield strength; and (3) an unstable regime where the system fluctuates in periodic fashion between the two stable regimes.

[84] Our parametric studies show that periodic behavior can be anticipated under a wide range of magmatic system conditions. The period is sensitive to several parameters including magma chamber size, conduit diameter, volatile content, temperature, rheological properties (expressed by a function that relates crystal content to yield strength and viscosity), and kinetic controls on crystallization. Changes in parameters with time during an eruption can result in changes in period of oscillations, in relative duration of the periods with high and low discharge and in the peak discharge rates. There can also be a transition between episodes of periodic behavior and episodes of steady stable discharge. Yield strength at high crystallinities can result in pulses of magma discharge that alternate with longer periods of zero discharge, while magma chamber pressure builds up to overcome the yield strength. As summarized in the introduction and briefly in the result sections, these

various kinds of behaviours are common in well-documented dome eruptions with comparable timescales of weeks to years. At leading order our models provide a suitable framework of theory to interpret dome-forming eruptions.

[85] Our models also indicate that magmatic systems in lava dome eruptions can be very sensitive to small changes in parameters. This sensitivity is most marked when the system is close to the cusps of the steady state solution. If discharge rate becomes so high that gas cannot escape efficiently during magma ascent, then conditions for explosive fragmentation can arise. Thus explosive eruptions are possible in these circumstances. Empirical evidence suggests that conditions for explosive eruption arise when magma discharge rates reach around 10 m^3 s^{-1} or more in dome eruptions [*Jaupart and Allegre*, 1991; *Sparks*, 1997]. Calculations show the possibility of such high discharge rates for the system parameters typical of lava dome-building eruptions.

[86] We have illustrated sensitivity of results by varying only one parameter at a time on plots of chamber pressure and discharge rate. However, magmatic systems have many controlling parameters that may vary simultaneously. Further, some controlling parameters are likely to be interdependent (such as temperature, volatile content and phenocryst content, for example) and others may be independent (such as magma temperature and conduit dimensions). An eruption can be expected to move through n-parameter space, making simulation and its parameter depiction difficult. Our results are simplified, so system sensitivity and behavior in the real world may be yet more complex. A volcanic system may be quite predictable when it is within a stable regime, but may become inherently unpredictable when variations in the parameters move the system toward transition points and flow regime boundaries.

[87] Our simplified computer simulations capture some of the key behavioral variations in lava dome eruptions. We use the Soufrière Hills eruption to illustrate this aspect. Two features of the discharge rate data [*Sparks et al.*, 1998] have been perplexing: the marked increase in discharge rate in May 1997, and the sudden cessation of the dome growth in March 1998. In May 1997 the discharge rate increased, changing from an average of about 2.6 m^3 s^{-1} during the period January 1996 to May 1997 to an average of 7–8 m^3 s^{-1} during May 1997 to March 1998. The later episode involved prominent periodic behavior with 6–7 week cycles [*Voight et al.*, 1999; *Sparks and Young*, 2002]. From our study such marked changes can occur due to small changes in system properties that lead to a cusp in n-parameter space where there is a rapid jump to a new behavioral regime. The change in May 1997 was from a relatively steady output to periodic behavior, consistent with movement from the lower to the intermediate regime. A key point is that rapid changes in eruptive behavior do not require any large change in the magma system.

[88] Our simulations suggest several mechanisms to explain an abrupt transition from high discharge rates to no discharge, as occurred at the Soufrière Hills in March 1999 [*Sparks et al.*, 1998]. These mechanisms include the development of non-Newtonian properties in slowing ascending magma, and small changes in some parameter such as decrease in magma temperature, volatile content, conduit and cross-sectional area. Another possible cause of transition is the decline in magma chamber pressure. If, as seems to be the case here, the system is in the oscillatory regime, but with outflux being greater than influx to the chamber the average chamber pressure must decline with time. This moves the system along the intermediate regime toward the upper cusp with discharge rate tending to increase with time despite the waning chamber pressure. As pressure declines below the value at the upper transition point the system transfers to a regime with very low discharge rate or no discharge rate and the eruption reduces in intensity dramatically or stops. The system will also be affected by the variations in dome height [*Stasiuk et al.*, 1993] since increases in dome height reduce the driving pressure and the position of cusps is also sensitive to dome height [*Melnik and Sparks*, 1999, 2002]. The Soufrière Hills dome reached its greatest height in March 1998 and this could have been a key factor in the regime change.

[89] As in all complex systems there are many controlling parameters. Our models capture some of the key dynamics, but are still simplified in many respects so do not fully capture the real variations. Our models do not, for example, consider variations of the dome height, gas escape to surrounding rocks, rheological effects of the bubbles and time dependent changes in conduit diameter. Additional effects can be expected for domes fed by dykes where dyke width may be coupled to pressure through elastic deformations [*Lister and Kerr*, 1991]. Because the model remains 1-D lateral distribution of parameters cannot be studied. This includes: lateral pressure gradients, magma crystallization on the conduit walls, wall rocks melting or erosion, formation of shear zones and shear heating. The models also make simple assumptions that influx into the chamber from a deep source is a constant. We have considered water as the only volatile and the addition of other gas species (e.g., CO_2 and SO_2) would add further variability. There are large uncertainties in some parameters which are likely to be very strong controls, such as the rheological properties of high crystalline magmas and crystal growth kinetic parameters, notably at low pressures (<30 MPa) where experiments are very difficult to do [e.g., *Couch et al.*, 2003]. Some parameters, such as conduit geometry variation with depth, are highly uncertain. With so many parameters, good fits can be achieved by selecting plausible values for real systems. *Barmin et al.* [2002], for example, were able to reproduce the patterns of extrusion rate at Mount St Helens and Santiaguito quite accurately. However, such models are not unique, partly because the actual values of some parameters may be quite different to the assumed values and partly because of the model simplifications.

[90] The full simulation of any particular volcanic eruption in such a nonlinear and sensitive system may appear a hopeless task. However, some reduction in uncertainties will certainly help to make the models more realistic. Further experimental studies of crystallization kinetics and magma rheological properties at high crystallinities are among the most obvious topics for future research. Advances in understanding the controls on magma input into an open-system chamber would be beneficial, since the delicate balance between input and output is a prime control on periodic behavior.

[91] Further model development includes 2-D effects, elastic deformation effects in dyke-fed domes and coupling between magma chamber and conduit flow dynamics. Even with such improvements, large parameter uncertainties and modeling difficulties will remain. In such circumstances the logical approach will be to start quantifying the uncertainties and sampling from them to produce probabilistic outputs based on ensemble models where numerical models of the kind discussed here can be run many times. A future challenge for numerical models will also be to produce simulated outputs which compare in detail with observations, in particular time series of discharge rates.

[92] **Acknowledgments.** This work was supported by following grants: NERC (GR3/13020), EC INTAS (01-0106), EC MULTIMO, by the Russian Foundation for Basic Research (RFBR 02-01-00065) and by the grant of President of Russian Federation (MD-689.2004.1). RSJS acknowledges a Royal Society-Wolfson Award. We thank Barry Voight, Alexey Barmin, Francis Albarede, and Takehiro Koyaguchi for insightful comments and suggestions that helped improve and clarify this work.

References

Aris, R. (2000), *Elementary Chemical Reactor Analysis*, 352 pp., Dover, Mineola, New York.

Barmin, A., O. Melnik, and R. S. J. Sparks (2002), Periodic behavior in lava dome eruptions, *Earth Planet. Sci. Lett.*, *199*, 173–184.

Bingham, E. C. (1922), *Fluidity and Plasticity*, 215 pp., McGraw-Hill, New York.

Bonnefoi, C., A. Provost, and F. Albarede (1995), The 'Daly gap' as a magmatic catastrophe, *Nature*, *378*, 270–272.

Bonnefoi, C., A. Provost, and F. Albarede (1999), The thermochemical dynamics of magma chambers: a simple model, *J. Geophys. Res.*, *104*, 7103–7116.

Cashman, K., and J. Blundy (2000), Degassing and crystallization of ascending andesite and dacite, *Philos. Trans. R. Soc. London, Ser. A*, *358*, 1487–1513.

Cole, P., E. S. Calder, R. S. J. Sparks, A. B. Clarke, T. H. Druitt, S. R. Young, R. Herd, C. L. Harford, and G. E. Norton (2002), Deposits from dome-collapse and fountain-collapse pyroclastic flows at Soufrière Hills Volcano, Montserrat, in *The Eruption of the Soufrière Hills Volcano, Montserrat From 1995 to 1999*, edited by T. H. Druitt and B. P. Kokelaar, *Mem. Geol. Soc. London*, *21*, 231–262.

Couch, S., R. S. J. Sparks, and M. R. Carroll (2001), Mineral disequilibrium in lavas explained by convective self-mixing in open magma chambers, *Nature*, *411*, 1037–1039.

Couch, S., C. L. Harford, R. S. J. Sparks, and M. R. Carroll (2003), Experimental constraints on the conditions of formation of highly calcic plagioclase microlites at the Soufrière Hills Volcano, Montserrat, *J. Petrol.*, *44*, 1455–1475.

Denlinger, R. P., and R. P. Hoblitt (1999), Cyclic eruptive behavior of silicic volcanoes, *Geology*, *27*(5), 459–462.

Druitt, T. H. et al. (2002) Episodes of cyclic Vulcanian explosive activity with fountain collapse at Soufrière Hills volcano, Montserrat, in *The Eruption of the Soufrière Hills Volcano, Montserrat From 1995 to 1999*, edited by T. H. Druitt and B. P. Kokelaar, *Mem. Geol. Soc. London*, *21*, 263–279.

Fedotov, S. A., V. N. Dvigalo, N. A. Zharinov, V. V. Ivanov, N. I. Seliverstov, S. A. Khubunaya, Y. V. Demyanchuk, L. G. Markov, L. G. Osipenko, and N. P. Smelov (2001), The eruption of Shiveluch volcano on May–July 2001, *Volcanol. Seismol.*, *6*, 3–15.

Hammer, J. E., and M. J. Rutherford (2002), An experimental study of the kinetics of decompression-induced crystallization in silicic melt, *J. Geophys. Res.*, *107*(B1), 2021, doi:10.1029/2001JB000281.

Harris, A. J. L., W. I. Rose, and L. P. Flynn (2002), Temporal trends in Lava Dome extrusion at Santiaguito, 1922–2000, *Bull. Volcanol.*, *65*, 77–89.

Hess, K. U., and D. B. Dingwell (1996), Viscosities of hydrous leucogranite melts: A non-Arrhenian model, *Am. Mineral.*, *81*, 1297–1300.

Hoblitt, R. P., E. W. Wolfe, W. E. Scott, M. R. Couchman, J. S. Pallister, and D. Javier (1996), The preclimactic eruptions of Mount Pinatubo, June 1991, in *Fire and Mud: Eruptions and Lahars of Mount Pinatubo, Philippines*, edited by C. G. Newhall and R. S. Punongbayan, pp. 457–511, Univ. of Wash. Press, Seattle.

Hort, M. (1998), Abrupt change in magma liquidus temperature because of volatile loss or magma mixing: Effects of nucleation, crystal growth and thermal history of the magma, *J. Petrol.*, *39*, 1063–1076.

Huppert, H. E., and R. S. J. Sparks (1988), The generation of granitic magmas by intrusion of basalt into continental crust, *J. Petrol.*, *29*, 599–624.

Huppert, H. E., and A. W. Woods (2002), The role of volatiles in magma chamber dynamics, *Nature*, *420*, 493–495.

Jaupart, C., and C. J. Allegre (1991), Gas content, eruption rate and instabilities of eruption regime in silicic volcanoes, *Earth Planet. Sci. Lett.*, *102*, 413–429.

Lister, J. R., and R. C. Kerr (1991), Fluid mechanical models of crack propagation and their application to magma transport in dykes, *J. Geophys. Res.*, *96*, 10,049–10,077.

Loitsyansky, L. G. (1978), *Fluid and Gas Mechanics* (in Russian), 847 pp., Nauka, Moscow.

Massol, H., and C. Jaupart (1999), The generation of gas overpressure in volcanic eruptions, *Earth Planet. Sci. Lett.*, *166*, 57–70.

Matthews, S. J., M. C. Gardeweg, and R. S. J. Sparks (1997), The 1984 to 1996 cyclic activity of Lascar Volcano, northern Chile: Cycles of dome growth, dome subsidence, degassing and explosive eruptions, *Bull. Volcanol.*, *59*, 72–82.

Melnik, O. E. (2000), Dynamics of two- phase conduit flow of high-viscosity gas-saturated magma: Large variations of sustained explosive eruption intensity, *Bull. Volcanol.*, *62*, 153–170.

Melnik, O. E., and R. S. J. Sparks (1999), Non-linear dynamics of lava dome extrusion, *Nature*, *402*, 37–41.

Melnik, O., and R. S. J. Sparks (2002), Dynamics of magma ascent and lava extrusion at Soufrière Hills Volcano, Montserrat, in *The Eruption of the Soufrière Hills Volcano, Montserrat From 1995 to 1999*, edited by T. H. Druitt and B. P. Kokelaar, *Mem. Geol. Soc. London*, *21*, 153–171.

Murphy, M. D., R. S. J. Sparks, J. Barclay, M. R. Carroll, and T. S. Brewer (2000), Remobilization origin for andesite magma by intrusion of mafic magma at the Soufrière Hills Volcano, Montserrat, W. I.: A trigger for renewed eruption, *J. Petrol.*, *41*, 21–42.

Nakada, S., H. Shimizu, and K. Ohta (1999), Overview of the 1990–1995 eruption at Unzen Volcano, *J. Volcanol. Geotherm. Res.*, *89*, 1–22.

Navon, O., and V. Lyakhovski (1998), Vesiculation processes in silicic magmas, in *Physics of Explosive Eruptions*, edited by J. S. Gilbert and R. S. J. Sparks, pp. 27–50, Geol. Soc., London.

Newhall, C. G., and W. G. Melson (1983), Explosive activity associated with the growth of volcanic domes, *J. Volcanol. Geotherm. Res.*, *17*, 111–131.

Norton, G. E. et al. (2002), Pyroclastic flow and explosive activity of the lava dome of Soufrière Hills volcano, Montserrat, during a period of no magma extrusion (March 1998 to November 1999), in *The Eruption of the Soufrière Hills Volcano, Montserrat From 1995 to 1999*, edited by T. H. Druitt and B. P. Kokelaar, *Mem. Geol. Soc. London*, *21*, 467–482.

Pallister, J. S., R. P. Hoblitt, G. P. Meeker, R. J. Knight, and D. F. Siems (1996), Magma mixing at Mount Pinatubo: Petrographic and chemical evidence from the 1991 deposits, in *Fire and Mud: Eruptions and Lahars of Mount Pinatubo, Philippines*, edited by C. G. Newhall and R. S. Punongbayan, pp. 687–731, Univ. of Wash. Press, Seattle.

Petford, N. (2003), Rheology of granitic magmas during ascent and emplacement, *Annu. Rev. Earth. Planet. Sci.*, *31*, 399–427.

Scott, S. K. (1994), *Oscillations, Waves and Chaos in Chemical Kinetics*, 96 pp., Oxford Univ. Press, New York.

Slezin, Y. B. (1984), Dispersion regime dynamics in volcanic eruptions. 2. Flow rate instability conditions and nature of catastrophic explosive eruptions, *Vulkanol. Seismol.*, *1*, 23–35.

Slezin, Y. B. (2003), The mechanism of volcanic eruptions (a steady state approach), *J. Volcanol. Geotherm. Res.*, *122*, 7–50.

Sparks, R. S. J. (1997), Causes and consequences of pressurization in lava dome eruptions, *Earth Planet. Sci. Lett.*, *150*, 177–189.

Sparks, R. S. J., and S. R. Young (2002), The eruption of Soufrière Hills volcano, Montserrat (1995–1999): Overview of scientific results, in *The Eruption of the Soufrière Hills Volcano, Montserrat From 1995 to 1999*, edited by T. H. Druitt and B. P. Kokelaar, *Mem. Geol. Soc. London*, *21*, 45–69.

Sparks, R. S. J., et al. (1998), Watts Magma production and growth of the lava dome of the Soufrière Hills Volcano, Montserrat, West Indies: November 1995 to December 1997, *Geophys. Res. Lett.*, *25*, 3421–3424.

Sparks, R. S. J., M. D. Murphy, A.-M. Lejeune, R. B. Watts, J. Barclay, and S. R. Young (2000), Control on the emplacement of the andesite lava dome of the Soufriere Hills Volcano, Montserrat by degassing-induced crystallization, *Terra Nova*, *12*, 14–20.

Stasiuk, M., C. Jaupart, and R. S. J. Sparks (1993), On the variations of flow rate in non-explosive lava eruptions, *Earth Planet. Sci. Lett.*, *114*, 505–516.

Stix, J., et al. (1997), A model for vulcanian eruptions at Galeras volcano, Colombia, *J. Volcanol. Geotherm. Res.*, *77*, 285–304.

Swanson, D. A., and R. T. Holcomb (1990), Regularities in growth of the Mount St. Helens dacite dome 1980–1986, in *Lava Flows and Domes:*

Emplacement Mechanisms and Hazard Implications, edited by J. H. Fink, pp. 3–24, Springer, New York.

Voight, B., R. P. Hoblitt, A. B. Clarke, A. B. Lockhart, A. D. Miller, L. Lynch, and J. McMahon (1998), Remarkable cyclic ground deformation monitored in real-time on Montserrat, and its use in eruption forecasting, *Geophys. Res. Lett.*, *25*, 3405–3408.

Voight, B., et al. (1999), Magma flow instability and cyclic activity at Soufrière Hills Volcano, Montserrat, B. W. I., *Science*, *283*, 1138–1142.

Wallace, P. J., A. T. Anderson Jr., and A. M. Davis (1995), Quantification of pre-eruptive exsolved gas contents in silicic magmas, *Nature*, *377*, 612–616.

Watson, I. M., et al. (2000), The relationship between degassing and ground deformation at Soufriere Hills Volcano, Montserrat, *J. Volcanol. Geotherm. Res.*, *98*, 117–126.

Watts, R. B., R. S. J. Sparks, R. A. Herd, and S. R. Young (2002), Growth patterns and emplacement of the andesitic lava dome at Soufrière Hills Volcano, Montserrat, in *The Eruption of the Soufrière Hills Volcano, Montserrat From 1995 to 1999*, edited by T. H. Druitt and B. P. Kokelaar, *Mem. Geol. Soc. London*, *21*, 115–152.

Woods, A. W., and T. Koyaguchi (1994), Transitions between explosive and effusive eruption of silicic magmas, *Nature*, *370*, 641–645.

Wylie, J. J., B. Voight, and J. A. Whitehead (1999), Instability of magma flow from volatile-dependent viscosity, *Science*, *285*, 1883–1885.

Young, S. R., R. S. J. Sparks, W. P. Aspinall, L. L. Lynch, A. D. Miller, R. E. A. Robertson, and J. B. Shepherd (1998), Overview of the eruption of the Soufrière Hills volcano, Montserrat, 18 July 1995 to December 1997, *Geophys. Res. Lett.*, *25*, 3389–3392.

O. Melnik, Institute of Mechanics, Moscow State University, 1, Michurinskii prosp., Moscow, Russia, 119192. (melnik@imec.msu.ru)

R. S. J. Sparks, Department of Earth Sciences, University of Bristol, Wills Memorial Building, Queen's Road, Bristol BS8 1RJ, UK.